Long-Baseline Neutrino Experiment (LBNE) Project

Conceptual Design Report

Volume 3: Detectors at the Near Site

September 10, 2012

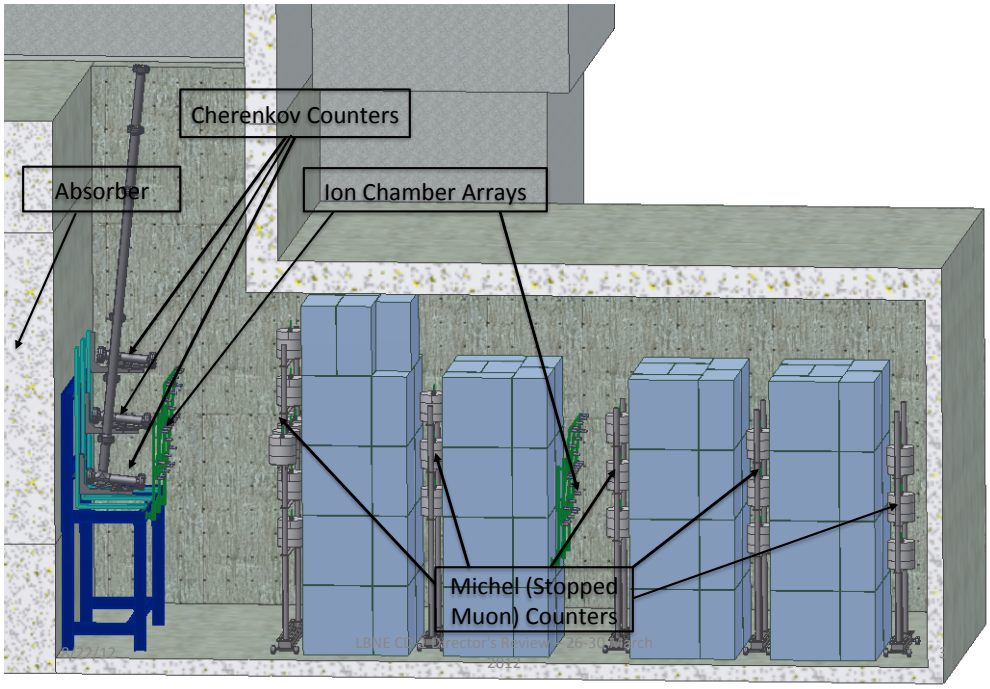

Contents

Acronyms, Abbreviations and Units

ADC	analog-to-digital converter
ASIC	application-specific integrated circuit
B-GDAQ	beamline global data acquisition
BEB	back-end board
BLM	beamline-measurement system
CC	charged current (interaction)
CCQE	charged current quasi-elastic (interaction)
CDR	Conceptual Design Report
CERN	European Organization for Nuclear Research
CNGS	Neutrino Beam to Gran Sasso (at CERN)
CP	charge parity
DAQ	data acquisition
DOE	Department of Energy
DUSEL	Deep Underground Science and Engineering Laboratory
ECAL	electromagnetic calorimeter
ESH	Environment, Safety and Health
eV	electron-Volt, unit of energy (also keV, MeV, GeV, etc.)
FEB	front-end board
FGT	Fine-Grained Tracker
FPGA	field-programmable gate array

FRA	Fermi Research Alliance
g-2	the New Muon g-2 Experiment at Fermilab
GDAQ	global data acquisition
GPS	Global Position System
HEP	high energy physics
ICARUS	Imaging Cosmic And Rare Underground Signals (experiment at LNGS)
K2K	"From KEK to Super–Kamiokande," long-baseline neutrino-oscillation experiment
LANL	Los Alamos National Laboratory
LAr	liquid argon
LAr-FD	(LBNE) Liquid Argon Far Detector
LArTPC	Liquid Argon Time Projection Chamber
LArTPCT	Liquid Argon Time Projection Chamber Tracker system
LBNE	Long-Baseline Neutrino Experiment
LHC	Large Hadron Collider (at CERN)
LNGS	Gran Sasso National Laboratory
m	meter (also nm, micron, mm, cm, km)
M-GDAQ	master global data acquisition
MicroBooNE	A 100-ton LArTPC located along Fermilab's Booster neutrino beamline
MINERvA	A neutrino-scattering experiment that uses the NuMI beamline at Fermilab
MiniBooNE	Booster Neutrino Experiment (at Fermilab)
MINOS	Main Injector Neutrino Oscillation Search experiment at Fermilab
MIPP	Main Injector Particle Production Experiment (at Fermilab)
MPPC	multi-pixel photon counter
MuID	muon-identification detector
N-GDAQ	neutrino global data acquisition

NA61	NA61/SHINE, experiment at CERN that studies hadron production in hadron-nucleus and nucleus-nucleus collisions
NC	neutral current (interaction)
ND	(Near Site) neutrino detector
NDC	Near Detector Complex; refers to the L2 Project under LBNE
NOMAD	Neutrino Oscillation Magnetic Detector, experiment at CERN
NOvA	NuMI Off-Axis Neutrino Appearance experiment at Fermilab
NuMI	Neutrino beam to MINOS
P5	Particle Physics Project Prioritization Panel
PMT	photomultiplier tube
QE	quasi-elastic (interaction)
STT	straw-tube tracker
Super-K	Super-Kamiokande, a neutrino detector in Japan
SURF	Sanford Underground Research Facility (in Lead, S.D., the LBNE Far Site)
T	Tesla; unit of magnetic field strength
T2K	Tokai-to-Kamioka, a long-baseline neutrino oscillation experiment in Japan
T2K ND280	Near Detector of the Tokai-to-Kamioka (T2K) experiment, located 280m from the beamline target
TDC	time-to-digital converter
TFB	T2K front-end board
TPC	time projection chamber
TR	transition radiation
TRIP-t	Trigger and Pipeleine with timing (full custom ASIC designed at Fermilab)
UA1	Experiment at CERN that ran from 1986 to 1993
UV	ultra-violet
V	Volt

W	watt (also mW, kW, MW)
WBS	Work Breakdown Structure
WLS	wavelength shifter

List of Figures

List of Tables

1 Introduction

1.1 Introduction to the LBNE Project

The Long-Baseline Neutrino Experiment (LBNE) Project team has prepared this Conceptual Design Report (CDR) which describes a world-class facility to enable a compelling research program in neutrino physics. The ultimate goal in the operation of the facility and experimental program is to measure fundamental physical parameters, explore physics beyond the Standard Model and better elucidate the nature of matter and antimatter.

Although the Standard Model of particle physics presents a remarkably accurate description of the elementary particles and their interactions, it is known that the current model is incomplete and that a more fundamental underlying theory must exist. Results from the last decade, revealing that the three known types of neutrinos have nonzero mass, mix with one another and oscillate between generations, point to physics beyond the Standard Model. Measuring the mass and other properties of neutrinos is fundamental to understanding the deeper, underlying theory and will profoundly shape our understanding of the evolution of the universe.

1.1.1 About this Conceptual Design Report

The LBNE Conceptual Design Report is intended to describe, at a conceptual level, the scope and design of the experimental and conventional facilities that the LBNE Project plans to build to address a well-defined set of neutrino-physics measurement objectives. At this Conceptual Design stage the LBNE Project presents a *Reference Design* for LBNE and alternative designs that are still under consideration for particular elements.

The scope includes

- an intense neutrino beam aimed at a far site
- detectors located downstream of the neutrino source

- a massive neutrino detector located at the far site
- construction of conventional facilities at both the near and far sites

The selected near and far sites are Fermi National Accelerator Laboratory (Fermilab), in Batavia, IL and Sanford Underground Research Facility (SURF), respectively. The latter is the site of the formerly proposed Deep Underground Science and Engineering Laboratory (DUSEL) in Lead, South Dakota.

This CDR is organized into six stand-alone volumes, one to describe the overall LBNE Project and one for each of its component L2 projects:

- Volume 1: The LBNE Project
- Volume 2: The Beamline at the Near Site
- Volume 3: Detectors at the Near Site
- Volume 4: The Liquid Argon Detector at the Far Site
- Volume 5: Conventional Facilities at the Near Site
- Volume 6: Conventional Facilities at the Far Site

Volume 1 is intended to provide readers of varying backgrounds an introduction to LBNE and to the following volumes of this CDR. It contains high-level information and refers the reader to topic-specific volumes and supporting documents, also listed in Section 1.1.5. Each of the other volumes contains a common, brief introduction to the overall LBNE Project, an introduction to the individual L2 project and a detailed description of its conceptual design.

1.1.2 LBNE and the U.S. Neutrino-Physics Program

In its 2008 report, the Particle Physics Project Prioritization Panel (P5) recommended a world-class neutrino-physics program as a core component of the U.S. particle physics program [1]. Included in the report is the long-term vision of a large detector at the formerly proposed Deep Underground Science and Engineering Laboratory (DUSEL) in Lead, S.D. (now SURF), and a high-intensity neutrino source at Fermilab.

On January 8, 2010, the Department of Energy (DOE) approved the Mission Need for a new long-baseline neutrino experiment that would enable this world-class program and firmly establish the U.S. as the leader in neutrino science. The LBNE Project is designed to meet this Mission Need.

With the facilities provided by the LBNE Project, the LBNE Science Collaboration proposes to mount a broad attack on the science of neutrinos with sensitivity to all known parameters in a single experiment. The focus of the program will be the explicit demonstration of leptonic CP violation, if it exists, by precisely measuring the asymmetric oscillations of muon-type neutrinos and antineutrinos into electron-type neutrinos and antineutrinos.

The experiment will result in precise measurements of key three-flavor neutrino-oscillation parameters over a very long baseline and a wide range of neutrino energies, in particular, the CP-violating phase in the three-flavor framework and the mass ordering of neutrinos. The unique features of the experiment – the long baseline, the broad-band beam, and the high resolution of the detector – will enable the search for new physics that manifests itself as deviations from the expected three-flavor neutrino-oscillation model. The scientific goals and capabilities of LBNE are outlined in Volume 1 of this CDR and the 2010 Interim Report of the Long-Baseline Neutrino Experiment Collaboration Physics Working Groups [2].

Siting the Far Detector deep underground, a scope opportunity that LBNE may seek to pursue in the future with non-DOE funding, would provide opportunities for research in additional areas of physics, such as nucleon decay and neutrino astrophysics, in particular, studies of neutrino bursts from supernovae occurring in our galaxy.

1.1.3 LBNE Project Organization

The LBNE Project Office at Fermilab is headed by the Project Director and assisted by the Project Manager, Project Scientist and Systems Engineer. Project Office support staff include a Project Controls Manager and supporting staff, a Financial Manager, an Environment, Safety and Health (ES&H) Manager, a Computing Coordinator, Quality Assurance, Procurement and Risk Managers, a documentation team and administrative support. The Project organization is shown in Figure 1–1.

The Beamline, Liquid Argon Far Detector and Conventional Facilities L2 Projects are managed by the Project Office at Fermilab, while the Near Detector Complex L2 Project is managed by a Project Office at Los Alamos National Laboratory (LANL).

More information on Project Organization can be found in Volume 1 of this CDR. A full description of LBNE Project management is contained in the LBNE Project Management Plan [3].

1.1.4 Principal Parameters of the LBNE Project

The principal parameters of the major Project elements are given in Table 1–1.

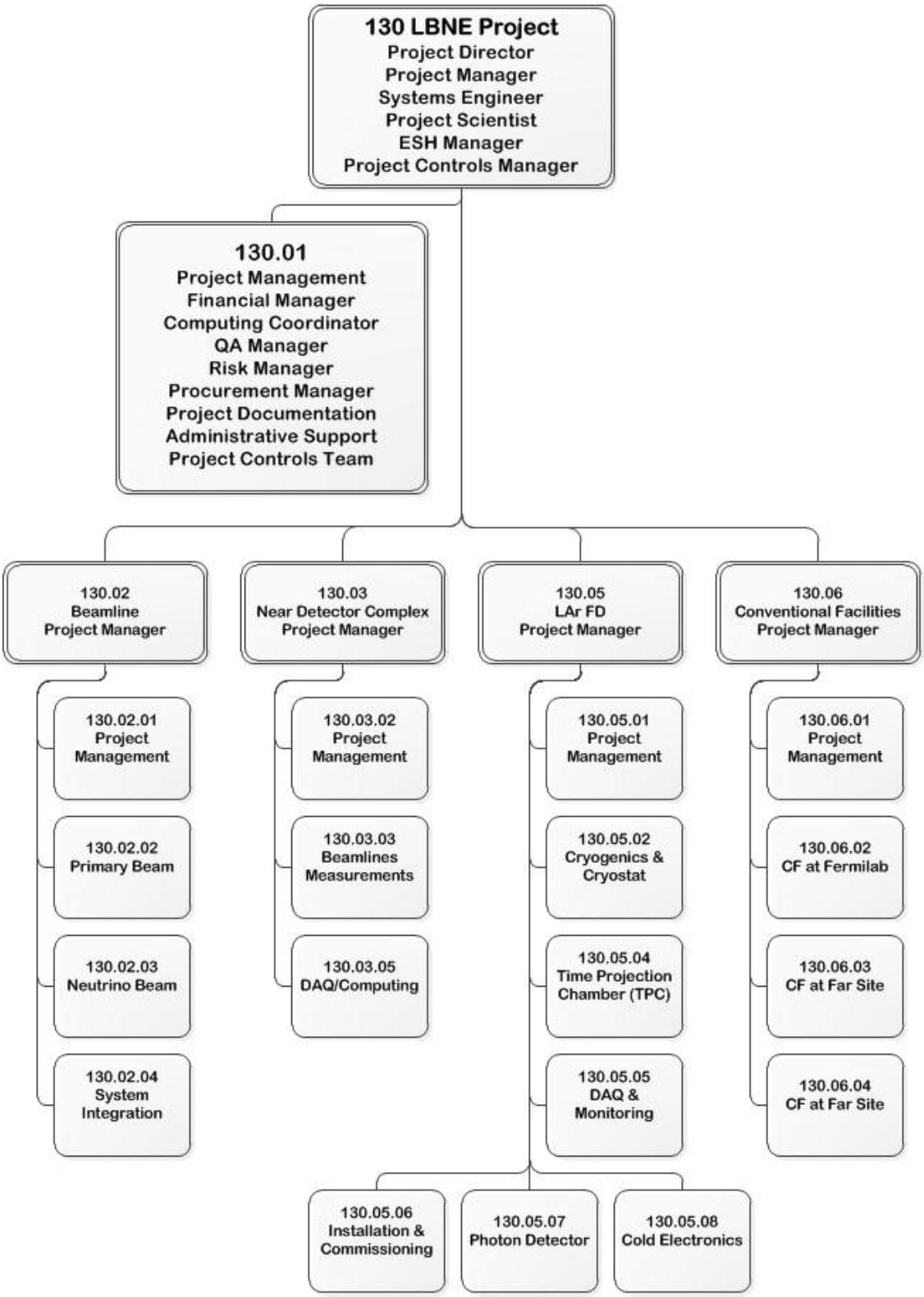

Figure 1–1: Organization chart for the LBNE Project (to WBS Level 3)

Table 1–1: LBNE Principal Parameters

Project Element Parameter	Value
Near- to Far-Site Baseline	1,300 km
Primary Proton Beam Power	708 kW, upgradable to 2.3 MW
Protons on Target per Year	6.5×10^{20}
Primary Beam Energy	60 – 120 GeV (tunable)
Neutrino Beam Type	Horn-focused with decay volume
Neutrino Beam Energy Range	0.5 – 5 GeV
Neutrino Beam Decay Pipe Diameter × Length	4 m × 203.7 m
Far Detector Type	LArTPC
Far Detector Active (Fiducial) Mass	13.5 (10) kton
Far Detector Depth	3 m overburden

1.1.5 Supporting Documents

A host of information related to the CDR is available in a set of supporting documents. Detailed information on risk analysis and mitigation, value engineering, ES&H, costing, project management and other topics not directly in the design scope can be found in these documents, listed in Table 1–2. Each document is numbered and stored in LBNE's document database, accessible via a username/password combination provided by the Project. Project documents stored in this database are made available to internal and external review committees through Web sites developed to support individual reviews.

Table 1–2: LBNE CD-1 Documents

Title	**LBNE Doc Number(s)**
Alternatives Analysis	4382
Case Study Report; Liquid Argon TPC Detector	3600
Configuration Management Plan	5452
DOE Acquisition Strategy for LBNE	5442
DOE Preliminary Project Execution Plan	5443
Integrated Environment, Safety and Health Management Plan	4514
LAr-FD Preliminary ODH Analysis	2478
LBNE Reconfiguration Final Report	Linked from LBNE web site (lbne.fnal.gov) under "Reports and Documents"
Global Science Objectives, Science Requirements and Traceback Reports	4772

Parameter Tables, Far Detector	3383
Preliminary Hazard Analysis Report	4513
Preliminary Security Vulnerability Assessment Report	4826
Procurement Plan	5329
Project Management Plan	2453
Project Organization Chart	5449
Quality Assurance Plan	2449
Report on the Depth Requirements for a Massive Detector at Homestake	0034
Requirements, Beamline	4835
Requirements, Far Detector	3747
Requirements, Far Site Conventional Facilities	4958
Requirements, Near Detectors	5579
Requirements, Near Site Conventional Facilities	5437
Risk Management Plan	5749
Value Engineering Report	3082
Work Breakdown Structure (WBS)	4219

1.2 Introduction to the LBNE Near Detectors (WBS 130.03)

LBNE will measure neutrino oscillations through high-statistics and high-precision measurements in the Far Detector. In order to achieve the ultimate neutrino-oscillation sensitivity, LBNE must be able to accurately and precisely predict signal and background events in the Far Detector.

The role of the LBNE Near Detector Complex (NDC) L2 Project is to minimize the systematic uncertainties on the long-baseline oscillation program and to thus maximize the oscillation-physics potential of the Far Detector. It is important that the Near Detectors not limit the sensitivity of the LBNE long-baseline neutrino-oscillation measurements. They should aid the analysis of electron-neutrino appearance, the primary oscillation channel, and muon-neutrino disappearance.

The NDC will be installed downstream of the LBNE beamline at Fermilab. The site is shown in Figure 1–2.

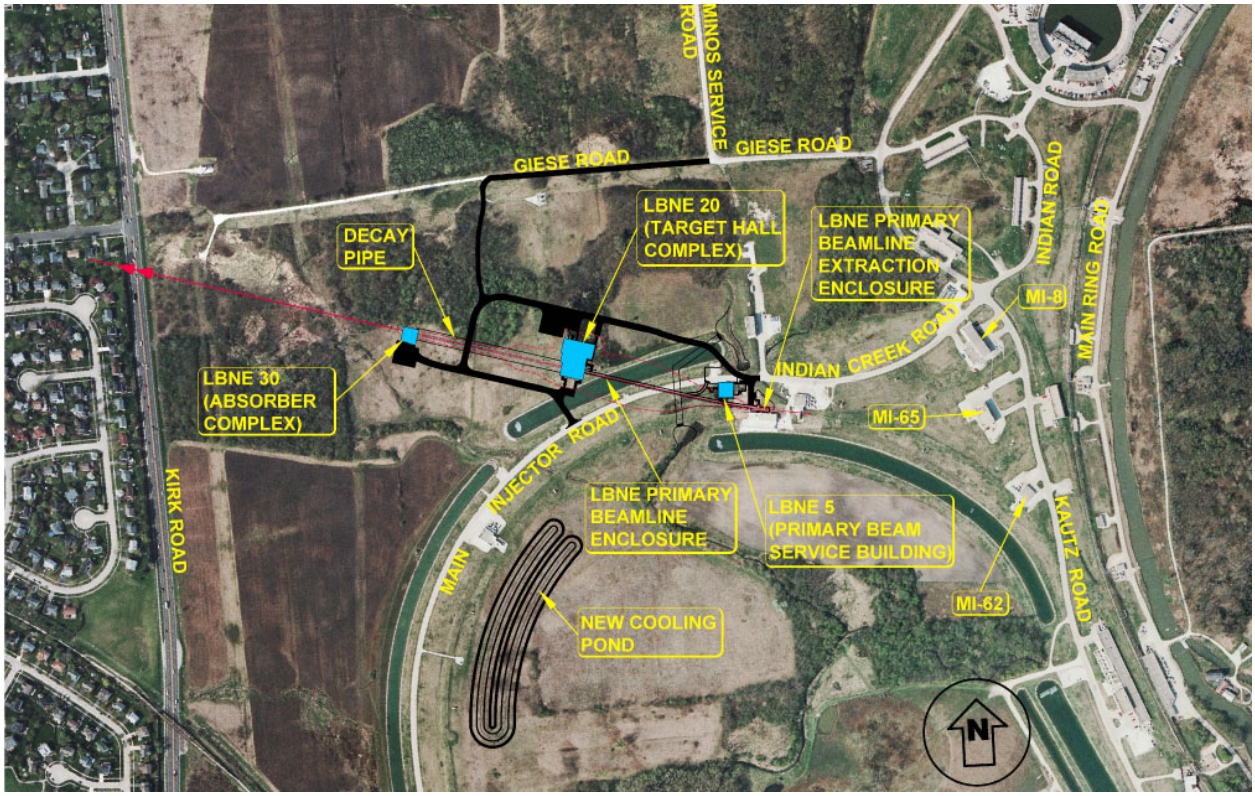

Figure 1–2: LBNE Overall Project Layout at Fermilab; NDC will be located near LBNE 30

Ideally, the NDC design would comprise both a beamline measurement system to determine neutrino fluxes and spectra, as well as near neutrino detectors to characterize the LBNE neutrino beam and the response of the Far Detector to those neutrinos. The characterization

would be sufficient to reduce the systematic errors on the predicted Far-Detector event rate (a function of neutrino oscillation parameters, e.g., θ_{13} and δ) to a level below expected statistical uncertainties. This would impose certain requirements on the accuracy with which the neutrino flux must be known at the Far Detector, since oscillations manifiest themselves as changes in the relative fluxes of the three neutrino flavors.

Due to financial constraints, this L2 Project has produced a conceptual design for only beamline measurement and data acquisition systems, discussed in Chapters 2 and 3, respectively. That said, the traditional strategy in neutrino-oscillation experiments has been to measure the un-oscillated events in a near neutrino detector and to calibrate the simulation of the neutrino flux and detector response on the basis of those measurements. The current approach relies on measurements made outside the scope of LBNE to calibrate the detector response and flux simulations, and to relate those measurements to LBNE through the use of common simulation code and measurements of the tertiary muon flux in both locations with nearly identical measurement systems. These additional elements of the measurement strategy are discussed in Chapter 4.

1.2.1 Neutrino-Beam Measurement Strategy

The purpose of the LBNE Near Detector effort is to make a suite of measurements that characterize the LBNE neutrino beam and the response of the Far Detector to the neutrinos.

The neutrino-beam measurement strategy will be two-pronged. It will entail measurements of the Far Detector response to a known flux of neutrinos, presumably a neutrino beam similar in nature to the LBNE beam. It will also entail the development of a detailed beamline simulation supported by direct measurements of critical aspects of the beam, for example, a well-developed suite of hadron-production measurements. Validation of the simulation via measurements of the secondary beam, such as measurements of tertiary muons, will be essential.

It is also essential to maintain a direct connection between the neutrino measurements not performed in the LBNE beam and the LBNE beam simulation at all levels. In other words, the simulation code, target material, detector configuration and supporting tertiary-beam measurements must be common and must be validated for both beams.

NuMI is the only beamline similar enough to the LBNE beamline design to be a candidate for use in the measurements. The NuMI beam has been calibrated by measuring the event rate in the MINOS near detector under a number of different beam configuations, i.e., several horn currents and target positions. The result has been a reasonably well understood neutrino flux. Those neutrino measurements were also supported by the NuMI muon-system measurements, as least for the high-energy part of the neutrino beam where the NuMI muon monitors were sensitive.

LBNE is planning to install a new set of muon-measurement devices into the NuMI beam as part of its prototyping effort. These devices are designed to measure the spectrum of muons at lower energies, starting at 2 GeV, as they exit the absorber. This will enable sensitivity to pions, which produce neutrinos at energies above 2 GeV. The NuMI muon measurements will then be repeated at LBNE for a variety of beam configurations as was done in NuMI. The combined set of measurements, in addition to the NuMI neutrino measurements, should provide a sound basis for predicting event rates at the LBNE Far Detector. The prototype devices need to be tested in the NuMI muon alcoves prior to CD-2, as they represent the only measurement linking the NuMI beam, where the near-detector neutrino measurements are made, to the LBNE beam. Waiting until after CD-2 would introduce a risk associated with achieving the LBNE physics goals.

1.2.2 Reference Design Overview

The NDC reference design consists of a beamline-measurements system (BLM) and a Global Data Acquisition system (GDAQ).

The BLM will be located in the region of the Absorber Complex at the downstream end of the decay region to measure the muon fluxes from hadron decay, as shown in Figure 1–3. The absorber itself is part of the Beamline L2 Project and is discussed in Volume 2 of this CDR.

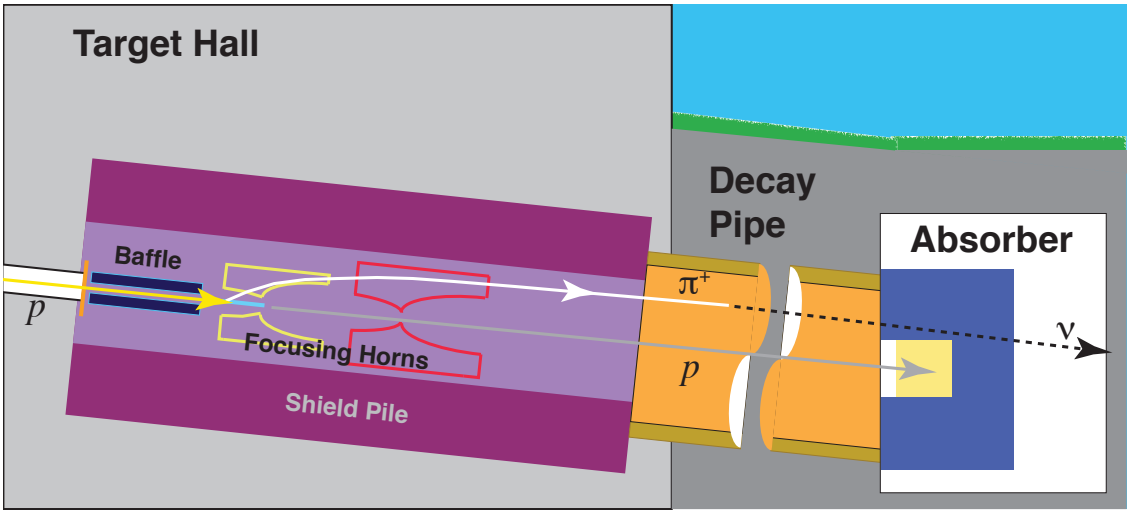

Figure 1–3: A cartoon of the LBNE neutrino beamline showing the major components of the neutrino beam. From left to right (the direction of the beam): the beam window, horn-protection baffle, target, the two toroidal focusing horns, decay pipe and absorber. The BLM system will be to the right of the absorber.

This BLM system is intended to determine the neutrino fluxes and spectra and to monitor the beam profile on a spill-by-spill basis, and will operate for the life of the experiment. Figure 1–

4 shows the downstream side of the absorber and a conceptual layout of the BLM muon systems. The first set of muon measurement devices, from left to right, are three variable-pressure, gas Cherenkov counters. Following these counters is the 5 × 5 ion-chamber array that is mounted directly to the rear wall of the absorber. Finally, there is a set of stopped-muon counters interspersed between walls of steel "blue blocks". The blue blocks provide several depths at which to monitor the muons as they range out and stop in the material.

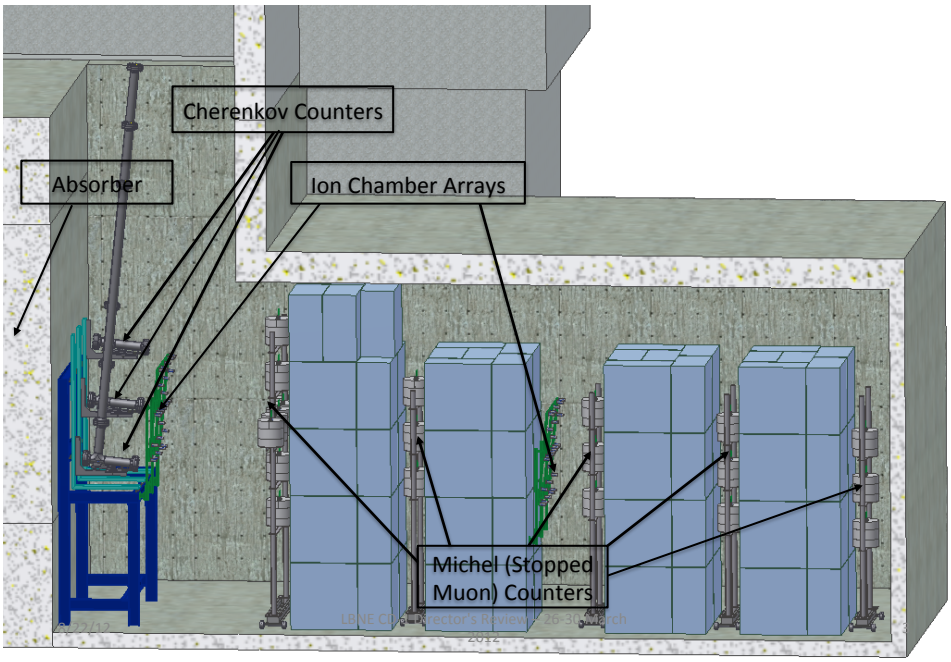

Figure 1–4: A model of the three muon monitor systems placed downstream of the absorber, in the muon alcove.

The GDAQ will collect raw data from each detector system in the NDC, issue global triggers, add timing data from a global position system (GPS) and build events.

1.3 Participants

The design for the LBNE Near Detector Complex (NDC) is being carried out by an LBNE L2 Project team, headed at Los Alamos National Laboratory (LANL) with participants from universities, in conjunction with outside contractors. The BLM are planned for construction at Fermilab.

The LBNE NDC is managed by the Level 2 Manager for the Near Detector Complex L2 Project. The supporting team includes a Level 3 Manager for each of the NDC's principal systems, Measurement Strategy, Beamline Measurement System, Global Data Acquisition and Computing. The organization is illustrated to WBS Level 4 in Figure 1–5.

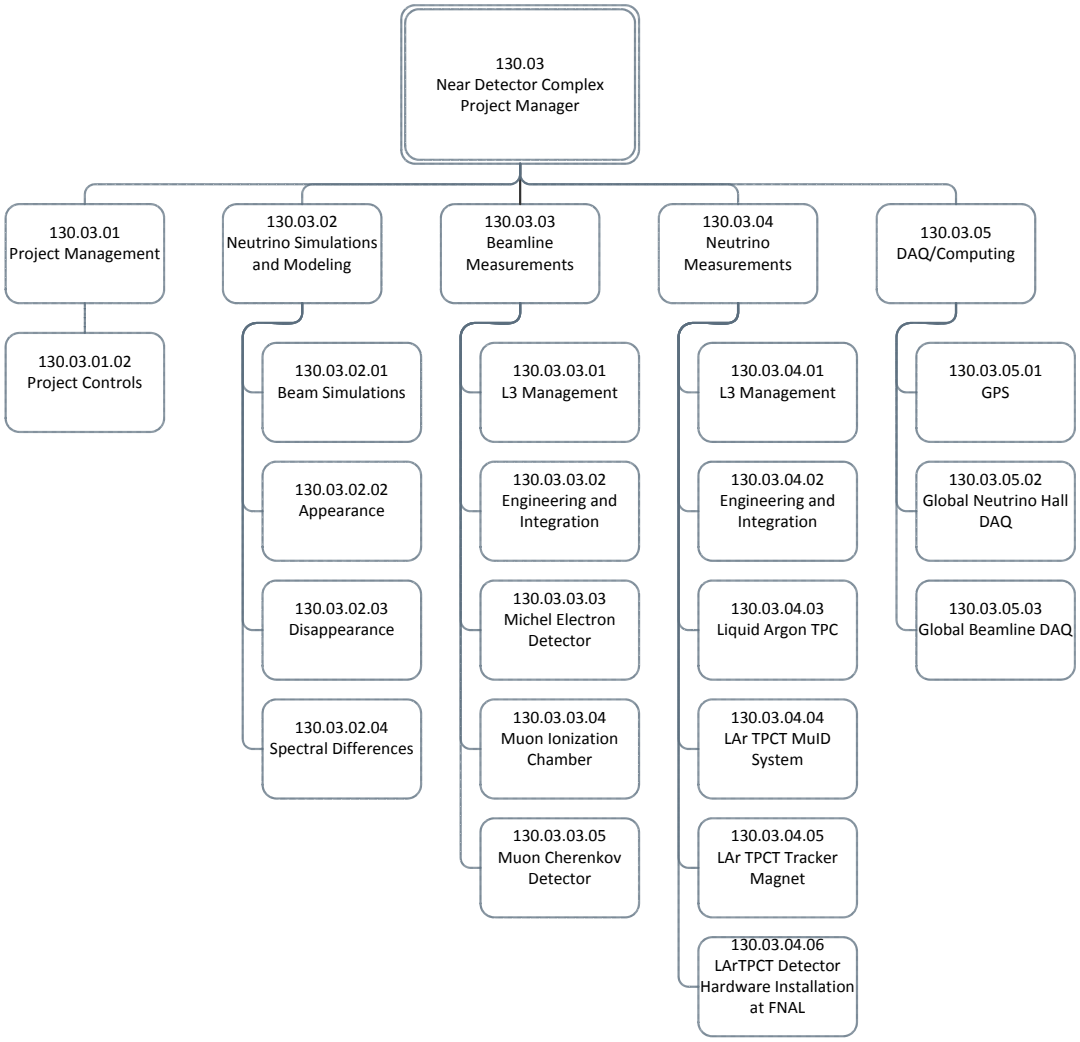

Figure 1–5: Organization chart for the NDC L2 Project (to WBS Level 4)

The Conventional Facilities Level 3 Near Site Manager is the LBNE Project liaison with the NDC L2 Project to ensure the L2 project civil requirements are met; this person is responsible for all LBNE conventional facilities scope at the Near Site.

Interaction between Fermilab facility engineers, LBNE NDC design teams, and design consultants consists of weekly telephone conferences, periodic design interface workshops, and electronic mail. An integration document resulting from these discussions will allow the NDC L2 Project team to coordinate activities and ensure that the design efforts remain on track to satisfy all requirements.

2 Near Detector Beamline Measurements (WBS 130.03.03)

2.1 Introduction

This chapter defines the LBNE strategy for measurements of secondary beam particles in the region behind the beam absorber. Those measurements are designed to provide constraints on the neutrino flux at the near and far detectors, and data on the pulse-to-pulse variation of the beam for beam diagnostic purposes. A description of equipment for monitoring the proton beam's interaction with the proton target can be found in Volume 2: The Beamline at the Near Site.

The measurements and apparatus described in this chapter fall into the catagory of equipment designed specifically for LBNE to detect muons exiting the decay tunnel.

2.2 Design Considerations

2.2.1 General

The requirements for the beamline measurements, as discussed in the NDC requirements documentation [4], are intimately related to how well the neutrino flux must be known. Given that LBNE does not have the luxury to construct identical Near and Far Detectors, a near-far comparison is more complicated than it was in the MINOS experiment [5], for example. While external hadron-production measurements can place strong constraints on the pion and kaon production in the target, they do not provide any confirmation of the simulation of other key features, such as the horn focusing, secondary interactions, and the pion scattering and absorption in the air-filled decay volume.

In addition to the external measurements, covered in Section 4, that confirm the simulation of the thick target, horn material, decay tunnel and absorber, it is desirable to constrain the

flux by making independent measurements at the 4–5% level of the muons that penetrate the absorber. It would not be practical to do this for all penetrating muons, but sufficient measurements at a few positions can be done in a cost-effective way.

2.2.2 Muon Measurements

The dominant, two-body decays of pions and kaons that produce neutrinos also result in the creation of daughter muons. Monitoring the muons exiting the decay volume can provide information about the direction, size, shape and flux of the neutrino beam. The daughter muon and neutrino energies in those two-body decays are completely anti-correlated. For example, a $\pi^+ \rightarrow \mu^+ \bar{\nu}_\mu$ decay will result in a $\bar{\nu}_\mu$ with an energy, E_ν, between zero and $0.43E_\pi$ plus a μ^+ with an energy of $E_\mu = E_\pi - E_\nu$ between $0.57E_\pi$ and E_π. This has the effect that the muon takes 79% of the pion energy on average, leaving the neutrino with only 21%. Thus, on average, the muon energy is 3.75 times that of the neutrino.

Because muons and neutrinos come from the same parent pion and kaon decays, a measurement of the absolute muon flux in conjunction with the energy spectrum seen in the muon monitors can confirm the absolute neutrino flux. The goal for the LBNE muon monitors is to determine the absolute muon flux to an accuracy of 5% above a muon energy of 6 GeV (which corresponds to a neutrino energy of 1.6 GeV) in the central part of the absorber. Figure 2–1 shows the total simulated neutrino flux at the Far Detector overlaid with the flux from only neutrinos having pion or kaon parents that contribute to the signal seen in the muon monitor. The simulation shows that between 3 GeV and 10 GeV, more than 90% of the neutrinos in the Far Detector come from this subset.

It is essential to monitor the stability of the beam direction over time. Figure 2–2 shows the effect on the muon-neutrino flux in the Far Detectors when the beam is misaligned by 0.4 mrad. For example, above 6 GeV, the ratio of the Far Detector flux over the Near Detector flux changes by 2%. To keep the change in the neutrino beam less than 1% in all energy bins, the beam direction must be known to a precision of approximately 0.2 mrad. Because the muon monitors will be located approximately 275 m from the beam target, this requires a measurement of the muons to an accuracy of approximately 5 cm.

The rate of muons crossing the monitors will be quite high, with preliminary LBNE beam simulations suggesting approximately 50 million muons per cm^2 for a pulse of 10^{14} protons-on-target. The muon monitors must also be capable of operating in a high-radiation environment. For example, the expected dose in the area downstream of the NuMI absorber is as high as 100 MRad per year [6].

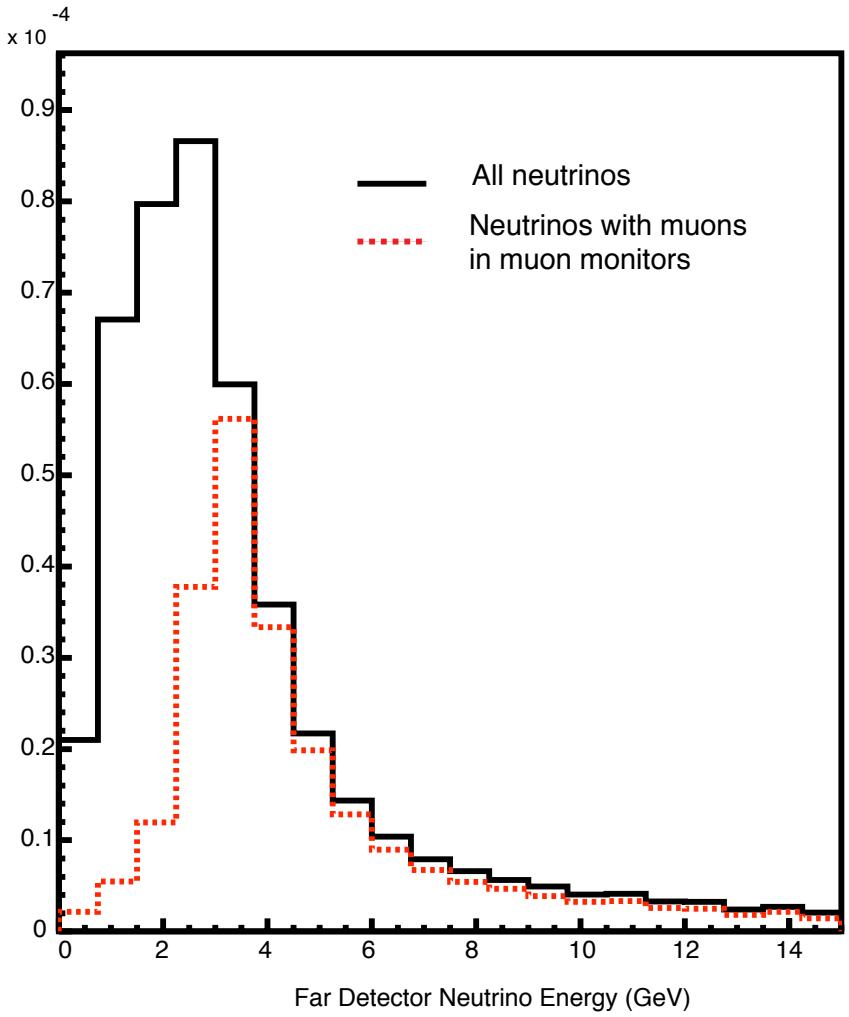

Figure 2–1: The total simulated neutrino flux at the Far Detector (black solid) overlaid with the neutrino flux, also at the Far Detector, coming from neutrinos with pion or kaon parents that contribute to the muon-monitor signal (red dashed), averaged over the back of the absorber. As shown in 2–8, the muon systems will probe down to 1.5 GeV in neutrino energy on the beam axis.

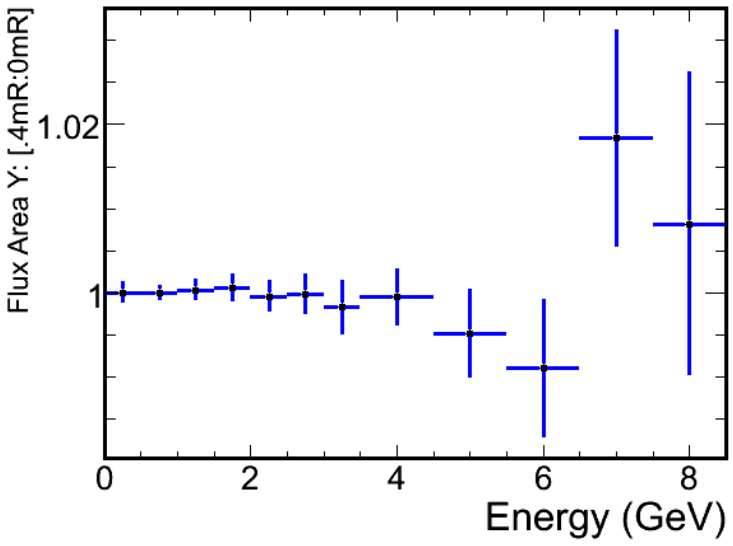

Figure 2–2: Ratio of the flux on-axis to the flux 0.4 mrad off-axis at the Far Detector position.

2.3 Muon-Measurement Facilities

The muon measurements are carried out in the region immediately following the hadron absorber at the end of the decay tunnel, below the Absorber Service Building (LBNE 30). An elevation view of the absorber area and the muon alcove is shown in Figure 2–3. The axis of the decay pipe cuts across the muon alcove at an angle, and the size of the alcove is largely determined by the requirement that it contain the shadow of the four-meter-diameter decay pipe, projected through the alcove, as shown by the blue lines in the elevation view of Figure 2–3.

Figure 1–4 shows the downstream side of the absorber and a conceptual layout of the muon systems described in various sections of this chapter. The absorber itself is encased in concrete. The first set of muon-measurement devices, from left to right, is a set of three variable-pressure gas Cherenkov counters, which are mounted directly to the rear wall of the absorber. Following that is an ion-chamber array and finally a set of stopped-muon counters which are interspersed between walls of steel "blue blocks". The blue blocks are there to provide several depths at which to monitor the stopped muons as they range out in the material. A second ion-chamber array will also be placed farther downstream within the blue blocks.

A perspective view of LBNE 30 is shown in Figure 2–4, and a detail of the lower level of Absorber Hall is given in Figure 2–5. The HV, water systems and gas systems for the muon monitors will be located nearby on the lower level. The readout electronics will be located in racks close to the surface.

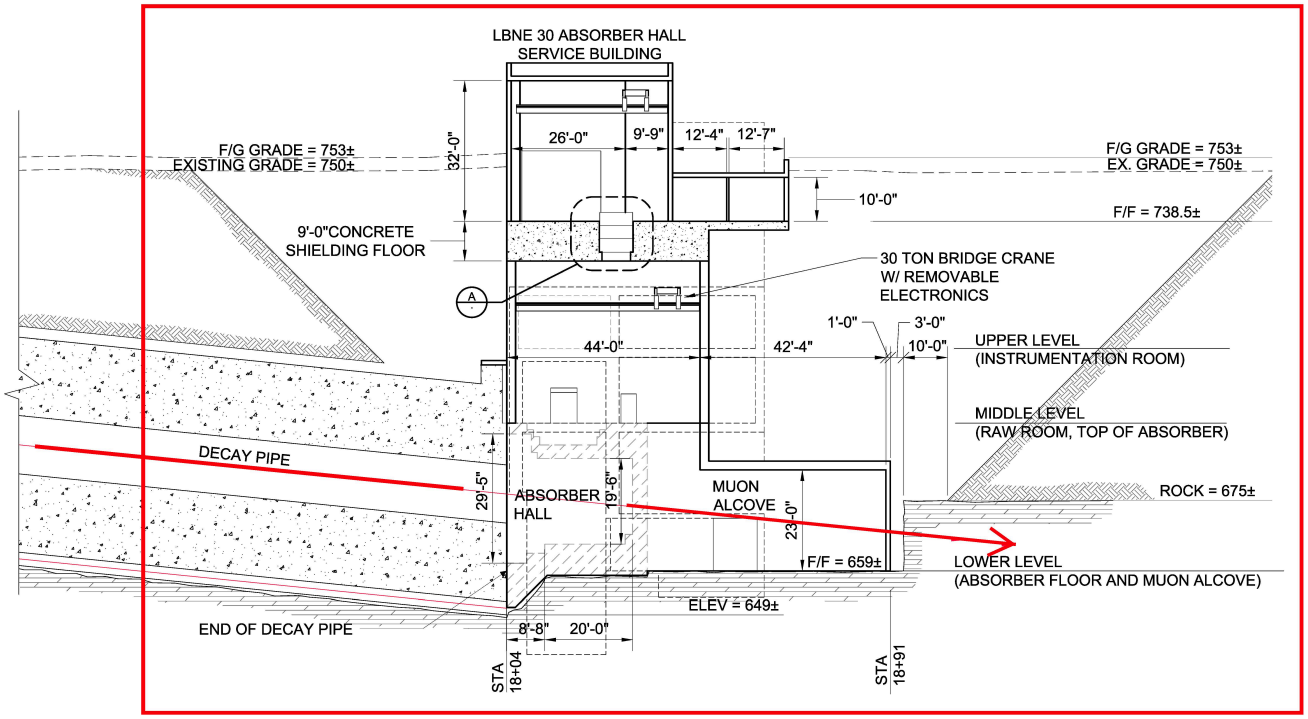

Figure 2–3: The Absorber Hall elevation view. The Absorber Service Building (LBNE 30) is on the surface and allows for crane access to the Absorber Hall. The muon alcove is directly behind the absorber.

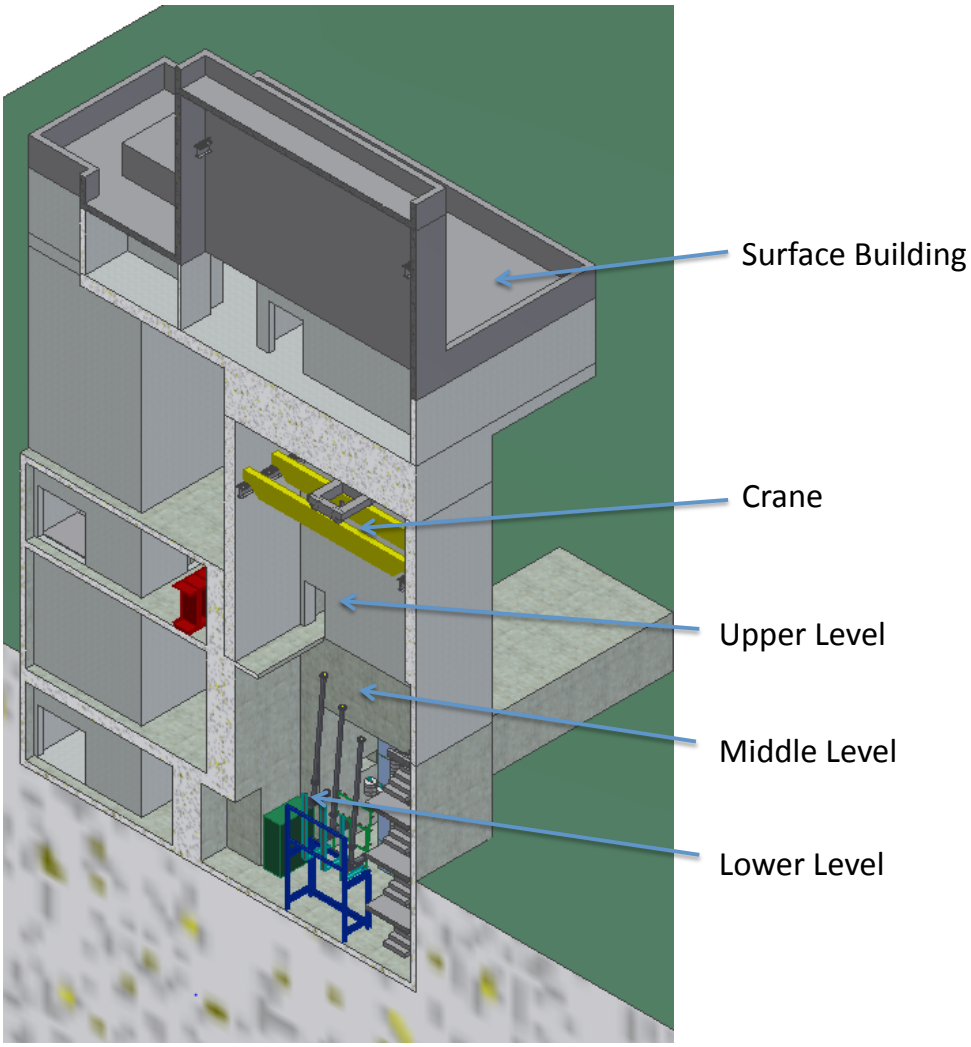

Figure 2–4: A perspective view of the Absorber Hall and LBNE 30.

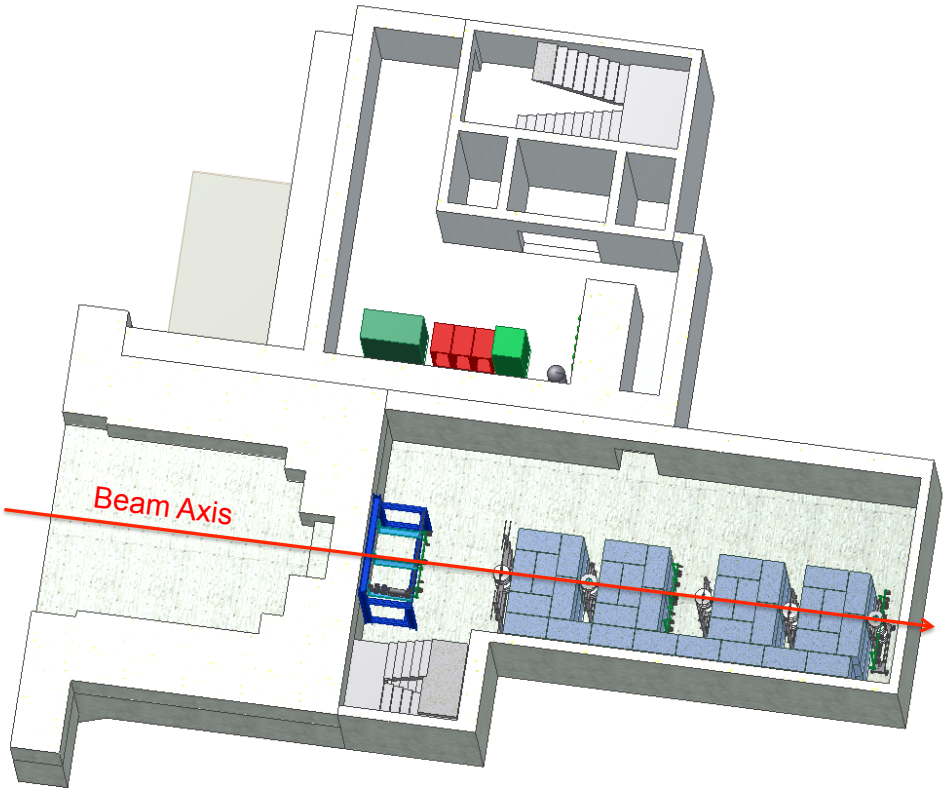

Figure 2–5: A perspective view of the Absorber Hall lower level.

It is important to have precise knowledge of the amount of material muons pass through before they are registered in the muon systems. The absorber itself is a complex, heterogeneous assembly of various materials. Figures 2–6 and 2–7 show the absorber conceptual design (more detail is available in Volume 2 of this CDR). A hole in the front side of the absorber, at left, is both surrounded and followed by the aluminum core of the absorber. The core is then surrounded by steel and standard steel "blue blocks", which are in turn surrounded by concrete. This complex geometry must be carefully understood and simulated in order to make the muon measurements effective.

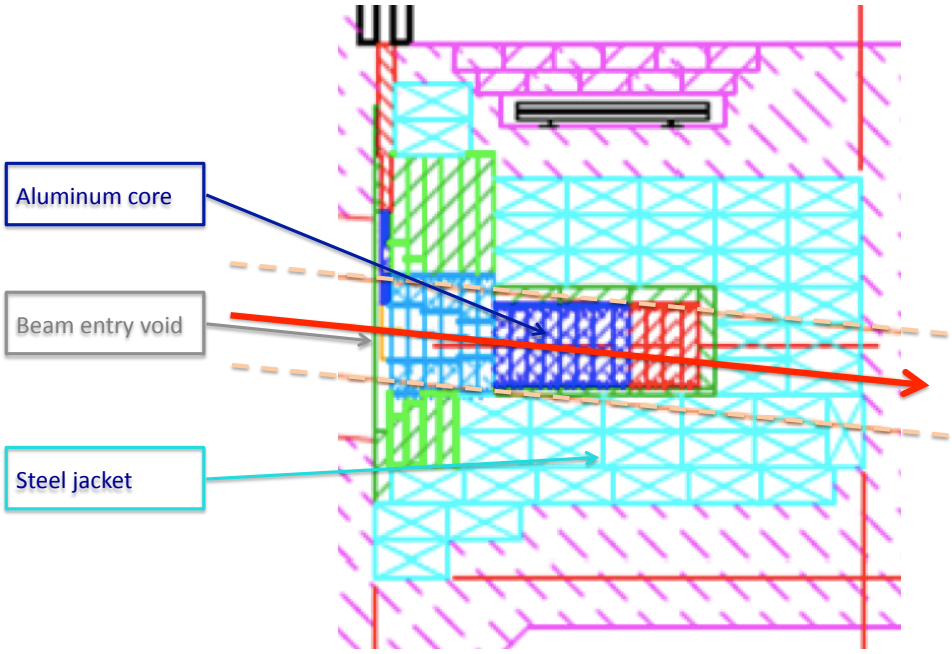

Figure 2–6: Absorber conceptual design. The figure shows the elevation view of the absorber at the end of the decay tunnel. The beam direction is shown by the red arrow. The absorber is constructed of several different materials as shown: aluminum (dark blue), concrete (magenta), and steel (other colors).

Figure 2–8 shows the energy lost by a horizontal muon as it traverses the absorber, as a function of the horizontal distance from the center. In the central region, out to a radius of roughly 50 cm, the muons lose roughly 5.6 GeV, so that the lowest-energy muons leaving the absorber at that point correspond to neutrino energies of $\sim$ 1.5 GeV. At a radius of roughly 70 cm, the full thickness of steel causes the muons to lose nearly 10 GeV, corresponding to neutrino energies of $\sim$ 2.6 GeV. From the perspective of the muon systems it will be desirable to lower these thresholds if possible. This might be accomplished by using more aluminum in the front part of the absorber. Of course the first concerns must be the containment of the radiation field induced by the proton beam, and the integrity of the absorber itself.

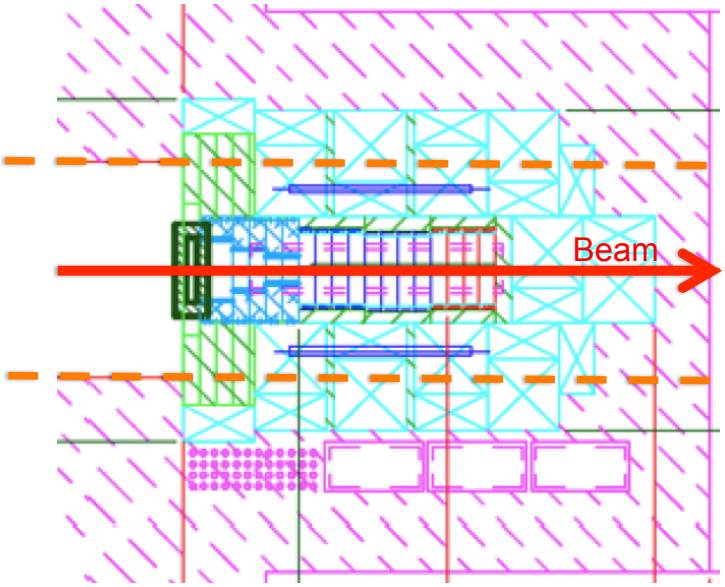

Figure 2–7: Absorber conceptual design, similar to Figure 2–6, that shows the plan view of the absorber.

2.4 Muon-Ionization Measurements

2.4.1 Introduction

Post-absorber muon measurements in most of the recent neutrino-beam experiments have typically employed a planar array of ionization counters to measure the muon profile and intensity. The NuMI beamline [6] and the K2K [7] [8] and T2K [9] [10] experiments have all utilized parallel-plate ionization chambers. These counters have been shown to work in the high-radiation environment.

K2K and T2K have also deployed solid-state silicon detectors [8] [11]. The advantage of silicon is that it is less sensitive to changes in the air temperature and pressure. However, these sensors are not as radiation-tolerant as the parallel-plate ionization chambers and will only be used in T2K for the initial beam operation.

One disadvantage to ionization counters is that they measure the total ionization deposited from all particle species (including the delta-ray electrons produced by the muons), making it challenging to convert the ionization signal into an absolute muon flux. The LBNE NDC plans to use the ionization counters to monitor the beam stability, direction and shape, but not to determine the absolute flux of muons or to determine the muon-energy spectrum. Instead, the stopped-muon counters and gas Cherenkov detector will be used, respectively, to determine the flux and energy spectrum of the muons.

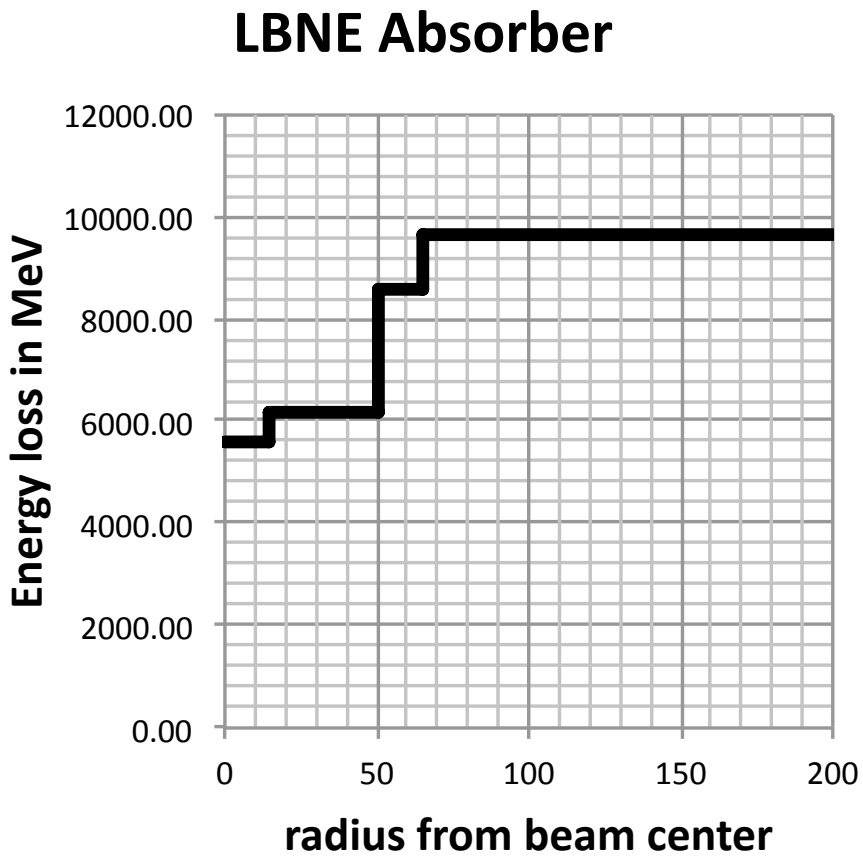

Figure 2–8: The absorber's approximate energy loss versus horizontal radius provides an indication of the variation in the depth of the absorber. Muons lose between 6 and 10 GeV depending upon where they cross the absorber.

2.4.2 Reference Design

The conceptual design for the LBNE muon-ionization chambers is similar to that used in NuMI, K2K and T2K. Due to their high radiation tolerance, sealed ionization counters are the default technology. For example, the CERN neutrino beam to Gran Sasso (CNGS) system uses an array of Large Hadron Collider (LHC) beam-loss monitors. For LBNE, it might be desirable to investigate solid-state devices besides silicon, such as diamond detectors (which are approximately an order of magnitude more radiation-tolerant than silicon counters [11][12]), to deploy as a cross-check of the gas ionization counters.

Figures 2–9 and 2–10 show the conceptual design for the ion-chamber array. Our conceptual design is based on commercial ion chambers made by LND, Inc. (model 50343). This chamber operates at 400 V and is designed to be sensitive to muons and insensitive to backgrounds such as neutrons. Radiation-hardened cables will be used to carry the signal to waveform digitizers, providing a complete spill-by-spill record of the muon beam.

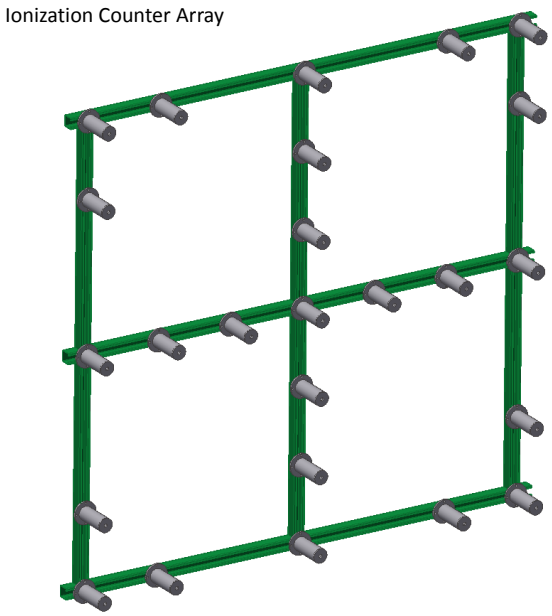

Figure 2–9: A model of the ion chamber layout on the back wall of the absorber showing the 7×7 grid configuration and supporting Unistrut rails.

The reference design for LBNE includes two layers of ionization counters, one behind the absorber and a second one behind steel shielding blocks. The chambers will be mounted in a 7×7 grid (with some missing elements), approximately two meters by two meters. LBNE wants to achieve a precision in the beam center of 0.2 milliradians (5 cm for a 250 m decay pipe). A quick study has determined the optimal arrangement of 25 ionization counters for each layer. For comparison, the NuMI monitor planes consist of a 9×9 array, and the T2K

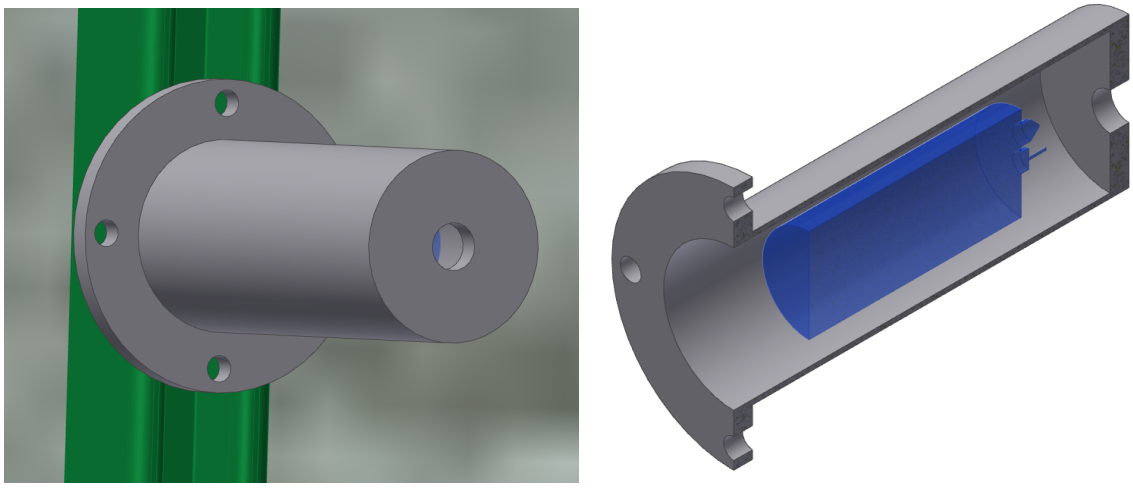

Figure 2–10: A model of the ion chamber housing and a section showing the commercial ion chamber inside the housing.

monitors use a 7 × 7 array of counters. The decision to use 25 counters for LBNE was motivated by a desire to see if a 7x7 array with some of the diagonal counters removed could achieve the desired sensitivity, thus reducing the total number of needed counters.

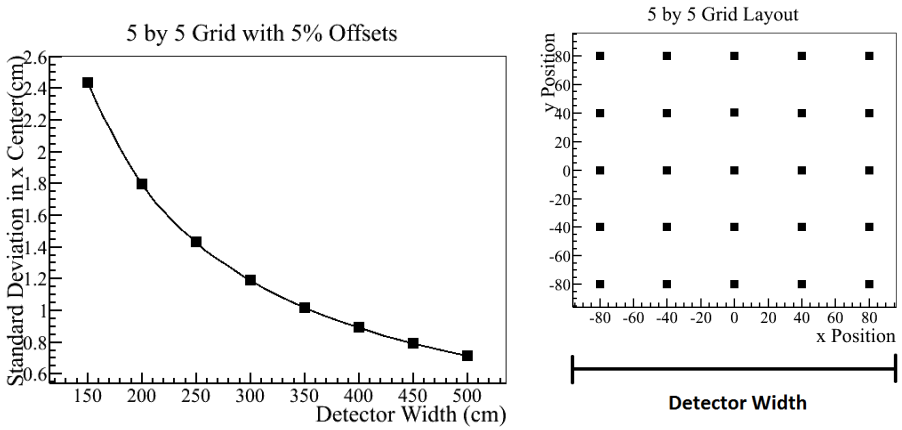

Figure 2–11: On the left: Precision as a function of detector width for a grid shaped detector with 5% random calibration offsets. On the right: The arrangement of ionization counters for the "5 by 5 grid" layout.

Several different designs for the counter arrangement were studied and the area covered by the detectors was varied. A toy Monte Carlo model was developed to estimate the precision of each design. The muon profile was assumed to be a Gaussian with a spread of 130 cm in the x and y dimensions and a center at the origin. The standard deviation on the beam center was studied as a function of array coverage for several designs and for 2%, 5% and 10% random systematic error offsets. Figure 2–11 shows the precision of the detector array

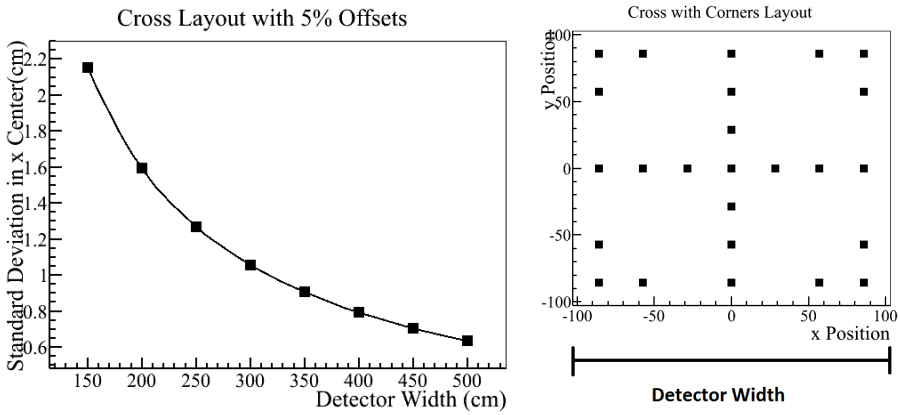

Figure 2–12: On the left: Precision as a function of detector width for a cross-shaped detector with 5% random calibration offsets. On the right: The arrangement of ionization counters for the "cross with corners" layout.

as a function of the width of the detector for a grid design and with 5% offsets. Figure 2–12 shows the same plot for a "cross with corners" layout.

The results show that the width of the detector array affects the precision more than the layout of the detectors. Increasing the array size improves the precision greatly. Concentrating the ionization counters to the outside of the layout gave the best precision for this simple model, but only by a small amount. Even for the layouts with 10% offsets and a width of 150 cm, the standard deviation on the beam center was less than our goal of 5 cm.

The LBNE muon ionization chamber design consists of two arrays of ionization counters, which is motivated by the NuMI target experience. As shown in Figure 2–13, over a period of several months, the number of events per proton on target gradually decreased over time, especially in the energy range from 2-4 GeV. This reduction in neutrino flux is attributed to target radiation damage. Figure 2–14 shows the ratio of the signal seen in the first muon alcove to the signal seen in the second muon alcove versus time. This ratio decreased in a similar manner over time. The first alcove was immediately after the absorber, while the second alcove was behind approximately 12 m of rock, and therefore saw only higher energy muons, since the lower energy ones would range out before reaching the second alcove. This gradual decrease in the ratio of the signals seen in these arrays was an indication of the target degradation and the relative reduction in the low-energy part of the neutrino and muon fluxes. *

It will be necessary to be able to monitor this ratio in LBNE on a spill-by-spill basis to look for signs of target degradation or horn failure. Therefore, a second ionization array, placed behind several layers of shielding blocks, will be necessary. In Figure 1–4 the second array is

*Similar trends were seen in the ratios of the other muon alcove signals, but the first/second ratio saw the largest effect.

placed behind 4 m of steel shielding. Since the density of steel is roughly 3 times larger than that of rock, this is comparable to the depth of the NuMI second muon alcove, which sits behind 12 m of rock. More detailed studies will need to be performed to determine if this is the optimal location for sensitivity to changes in the target density.

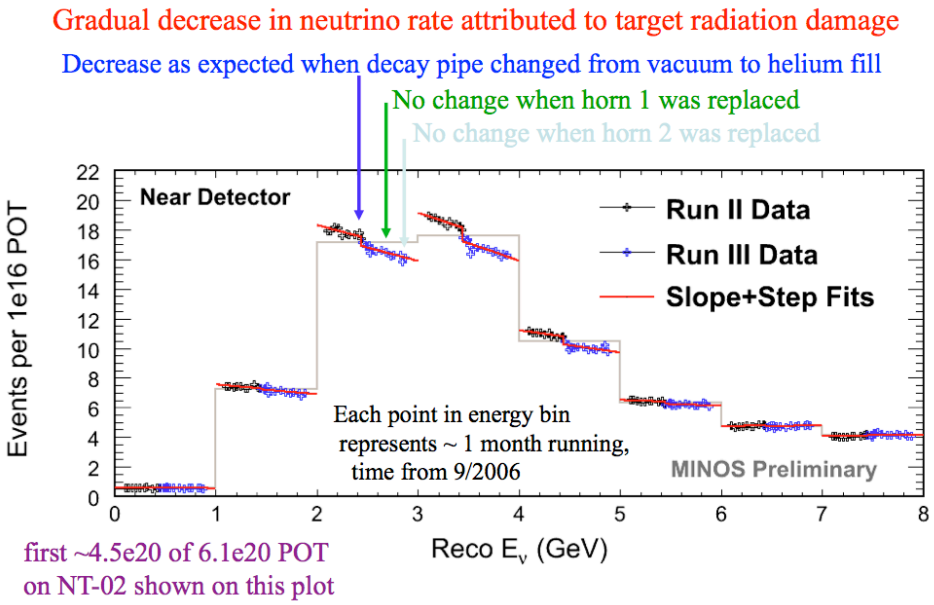

Figure 2–13: Shown here is the number of events observed in the MINOS near detector per proton on target. The horizontal axis is divided into energy bins. The gray line shows the average number of events in each energy slice over the whole time period. Within each energy bin each cross indicates the value in roughly one month of running, with time increasing to the right.

2.4.3 Prototype Design and Testing

For the gas ionization detectors, a small array of prototype counters can be built and potentially operated in the existing NuMI alcoves to determine the optimal design and operating conditions for the LBNE monitors. Ideally this could be done during the long shutdown for the NOvA upgrade that will end in Spring 2013. That will provide a good field test in roughly the same environment as expected during LBNE operations. It can also be cross-checked against the existing NuMI muon-monitoring system. The goals of these tests would be to understand the linearity of the response of these counters (by comparing the observed signal to variations in the beam intensity), their long-term stability and operational reliability.

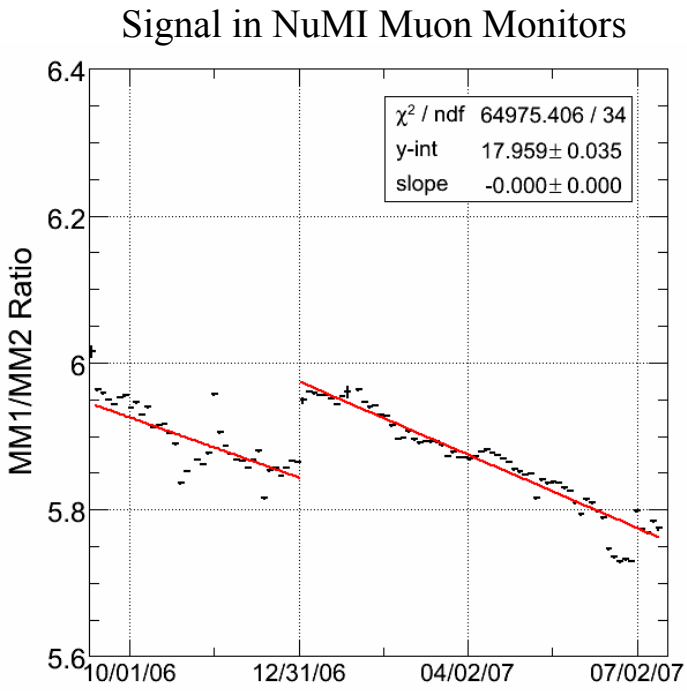

Figure 2–14: Shown here is the ratio of the signal seen in the NuMI first muon alcove over the signal seen in the second muon alcove over time. The step that occurs on approximately December 31, 2006 is when the NuMI decay volume was changed from vacuum to helium, and this change is expected to attenuate the higher energy muon flux more than the lower energy flux.

2.4.4 Installation

The system installation will begin following completion of the Absorber Hall and LBNE 30 and the installation of the stopped-muon counter system (described in Section 2.5).

2.4.5 Operation

The muon-monitor-system data will be displayed in the control room at the Absorber Hall upper level on a spill-by-spill basis to monitor the beam stability and look for potential signs of target or horn degradation. This control room will be accessible during the beam operation.

2.5 Stopped-Muon Detector

2.5.1 Introduction

An option being developed for measuring muons is stopped-muon counters, also called Michel-electron detectors. This method is still conceptual; however, in principle, it could measure the muon flux without suffering from some of the disadvantages intrinsic to systems that detect through-going muons. The strategy employed here is to stop muons in a material with significant carbon content and, via muon capture, to produce ^{12}B that will in turn undergo β decay. The high-carbon material, in this case graphite, surrounds a Cherenkov radiator material which is sensitive to electrons from muon decay or high-energy beta decays. Figure 2–15 shows a conceptualization of a single stopped-muon counter.

The detectors will only operate in the lower-rate environment that is present many microseconds after the beam pulse is over. There are two possible modes for this type of system. The first is an integrating mode where the characteristic decay time of 2.2 μs for muon decay and corresponding beta-decay lifetimes is used to unfold the total number of decays. The other mode under investigation uses the ability to record individual decays rather than an analog current measurement. This mode may allow a more precise absolute normalization of the flux and fit the muon lifetime in the Michel-electron detector. This will provide a more robust cross-check on the muon signal than will ionization detectors, which are sensitive to delta rays, photon conversions and other charged particles.

Although this technique has never been tried on a large scale, a small demonstration project in K2K was able to see Michel decays with a 10^3 signal/background ratio and to measure the absolute rate with 30% precision[12].

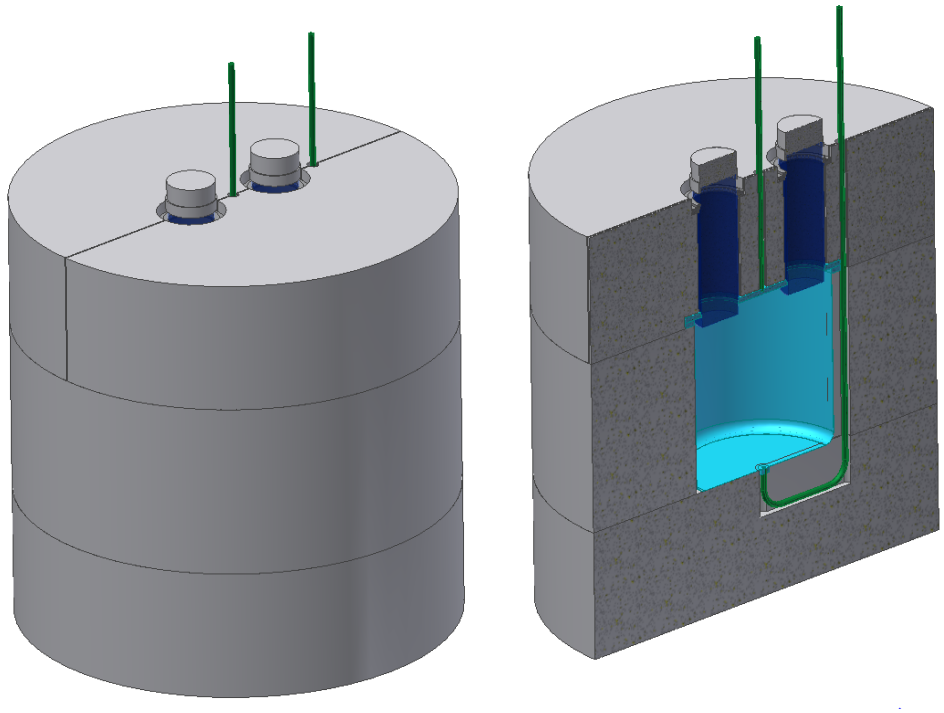

Figure 2–15: A conceptualization of a single Michel-electron detector (stopped-muon counter).

2.5.2 Reference Design

The stopped-muon detector reference design is modular and based on a Cherenkov radiator of minimum size to contain a 52.8-MeV electron and distinguish it cleanly from lower-energy radioactivity. This conceptual design employs a liquid H_2O radiator, although mineral oil and aerogel are other possible radiator materials. The radiator will be coupled to a photomultiplier tube (PMT) or other photon counter. Graphite has been chosen for the material surrounding the radiator as it provides the ^{12}C necessary for producing ^{12}B via muon capture. The entire module will be encased in a material that provides both a uniform-density stopping target for muons and some shielding from incoming neutrons. One or two signal channels will be associated with each module, and the full waveform from each channel over approximately 100 ms will be recorded on each beam pulse.

Approximately 9 modules will be placed just behind the absorber in a cross pattern. An additional 12 will be placed at multiple depths in the shielding in order to sample the muon flux from different energies, as shown in Figures 1–4 and 2–16. The shielding will simultaneously act to range out the muons and shield the detectors from neutrons. The Cherenkov light from Michel-decay electrons will exit the counter and be collected by either nearby PMTs or by a light guide which will guide the light to a remote optical sensor.

To probe the muon flux at lower energies, it may also be feasible and/or desirable to place some additional modules within the downstream part of the absorber or in the outermost radii of the decay-pipe shielding. The ability to do this may be limited, however, by the presence of muons from stopped, positively charged pion decays due to nearby hadron showers.

Besides the Michel decays of stopped muons, the system will independently measure both the μ^+ and μ^- stopped rates as a function of depth. While the 2.2 μs decay time of the μ^+ is a reliable signature, in graphite roughly 8.5% of the μ^- undergo capture on the ^{12}C nucleus, and 15% of those leave behind a ^{12}B ground state nucleus. That ^{12}B nucleus will undergo β decay with a half-life of 20.20 ms and an electron spectrum with an endpoint of 13 MeV. With a graphite layer around the detector, this signal is expected to yield a reliable measurement of the rate of stopped μ^-.

2.5.3 Prototype Development and Testing

Prototype development activity for the Michel-electron detectors will be divided into studies of the rate and radiation environment where the detectors will be located and development of the counters themselves.

The radiation environment will be studied both with Monte Carlo simultions and by measurements from initial prototype detectors in the NuMI muon alcoves [6]. Studies will be performed to determine if the photon sensors can survive the radiation environment at the

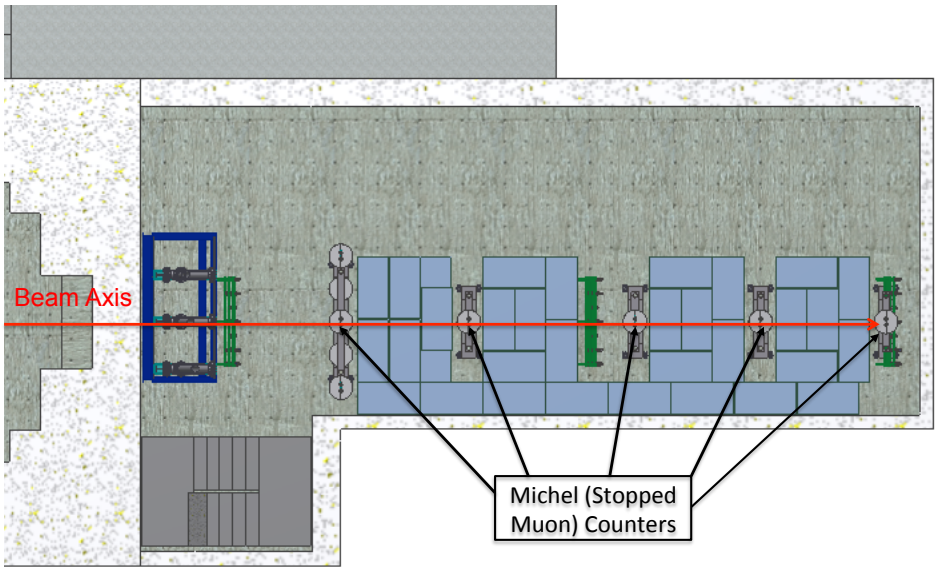

Figure 2–16: A top view of the lower level of the Absorber Hall showing a possible arrangement of "blue blocks" and Michel-decay detectors. In this case there is roughly 2 GeV of energy loss per wall of blue blocks. The counters can be moved between layers and within a single layer.

location of the Michel detector. If the sensors can survive, they can be attached directly to the Cherenkov medium; if not, optical guides will have to bring the light to a lower-radiation area to the side of the beam. Potential radiation damage to the Cherenkov radiator itself will also be studied.

The detector design will focus on selecting radiator and shielding material, photon-detection technology and control/readout hardware. Possible radiators include aerogel, which may be designed to be replaced periodically, and flowing liquids such as H_2O or mineral oil. Long-timescale saturation from the very high-rate environment of the beam spill could affect the photon-counting devices [13]. Thus, it will likely be necessary to design fast-switching, high-voltage circuits that turn on the photon counters in the first few microseconds after the spill is over. A similar system was developed in the 1990s for the Brookhaven Muon (g-2) Experiment [14] .

2.5.4 Installation

The stopped-muon counters will be installed after completion of the Absorber Hall and LBNE 30 and installation of the absorber. They will be placed into the spaces between the blue-block walls on support frames. There will be access to the areas between the shield blocks from the side, and the stopped-muon counters will be designed so that they can be wheeled in from the side. If needed, they could then be moved around to measure the stopped-muon

rates across the muon beam.

2.5.5 Operation

The muon-monitor-system data will be displayed in the control room on a spill-by-spill basis to monitor the beam stability. Because the system will be located in a radiation-controlled environment that will not be accessible during the beam operation, it is essential that the electronics be designed for remote operation.

2.6 Muon Cherenkov Detectors

2.6.1 Introduction

As mentioned in Section 2.2.2, one disadvantage of an ionization system for the muon monitors is that it measures the ionization due to all particles, including delta-ray electrons and neutrons. This makes it difficult to determine the muon flux. Furthermore, the ionization system is unable to measure the momentum distribution of the muons. To resolve this problem, T2K is considering the idea of deploying a Cherenkov counter downstream of the absorber. A Cherenkov counter deployed by LBNE will not image individual Cherenkov rings, but rather will see the integrated signal from many muons due to the very large instantaneous flux. In addition, by varying the radiator gas pressure, and hence the Cherenkov threshold, the system's index of refraction will vary, allowing it to map out the muon momentum distribution.

Figure 2–17 shows the expected distribution of velocities, β (v/c), for muons and electrons after exiting the absorber. Figure 2–18 shows the expected angle with respect to the beam for electrons and muons with similar velocities (implying that both are visible above the same Cherenkov threshold). Despite the similar velocities, the muons are much more likely than the electrons to be directed parallel to the beam.

Therefore, a detector that takes advantage of the directional nature of Cherenkov light will have less background contributions from electrons and other isotropic background particles such as neutrons, than will an ionization system, for example.

2.6.2 Reference Design

There are a number of possible designs for Cherenkov counters. The conceptual design is based on a traditional beamline Cherenkov counter, where a gas radiator is contained in a

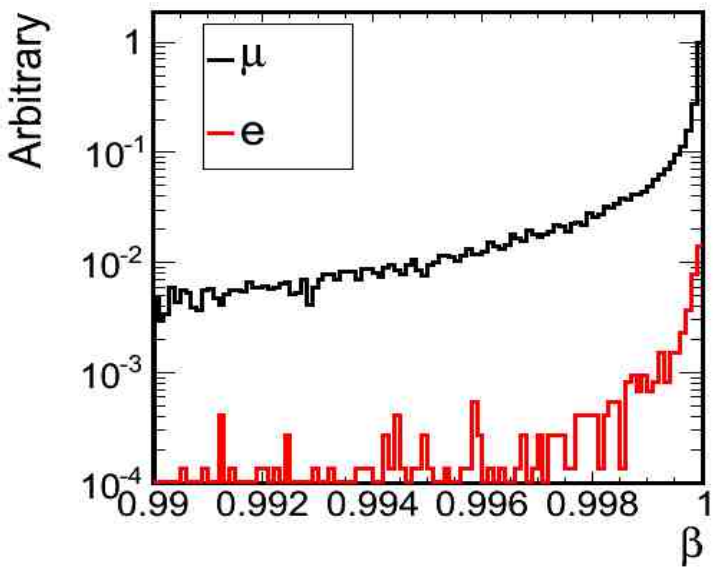

Figure 2–17: Simulated electron and muon velocities exiting the absorber. This plot is based on a simulation gnumi[15] of the LBNE beamline.

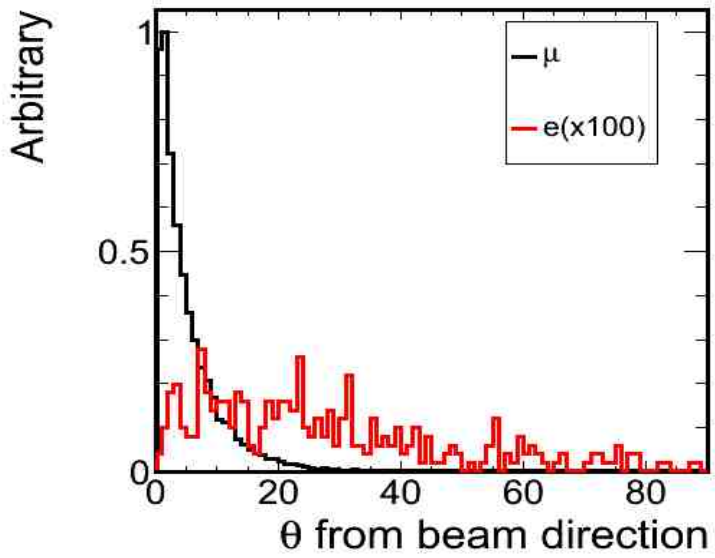

Figure 2–18: Simulated plot of angle with respect to the beam for electrons and muons exiting the absorber. This plot is based on a gnumi simulation of the LBNE beamline.

pressurized tube. The Cherenkov light in a narrow cone is collected at the end of the tube by a mirror that reflects the light 90 degrees towards a photosensor located outside the high-radiation field of the alcove. The gas pressure, varied from vacuum to several atmospheres, will determine the index of refraction, and hence the muon-momentum threshold. Several such tubes could be constructed in an array transverse to the beam direction. The resulting pressure scan will give the momentum distribution of the muons at an array of points across the end of the absorber.

Figure 2–19 shows conceptually how the Cherenkov system might be constructed. Safety considerations suggest that the diameter of the radiator tube and light-guide tube be six inches or less. A photosensor, located outside the direct radiation field of the muons, will view the primary mirror through a telescopic optical system.

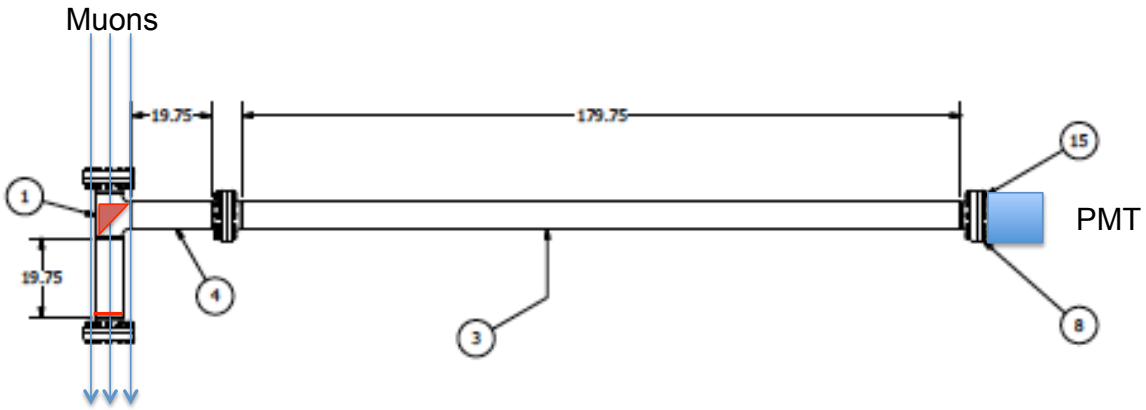

Figure 2–19: The Cherenkov counter conceptual design. Muons at threshold momentum emit forward Cherenkov light which is reflected via two flat mirrors (one at 90 degrees) to a PMT located outside of the muon radiation field.

The layout of the Cherenkov counter system is shown in Figure 2–20.

The preferred option is to use a gas Cherenkov system containing a noble gas with a high index of refraction, where the density of the gas can be varied to change the Cherenkov threshold. The noble gas will reduce potential degradation due to reactivity in the high radiation field of the post-absorber environment. Varying the pressure will provide more information about the momentum spectrum of the muons.

The combination of a flat mirror and a 90^0 mirror will reflect light out to a PMT. The UV-sensitive PMT will collect light from normal incidence on the primary mirror to $\sim$5 mrad. Figure 2–21 shows that, with a 5 mrad acceptance, the light yield per particle will be approximately one photon near threshold. That is more than ample light for the system where the particle flux is of order 10^8 per cm^2 on a PMT.

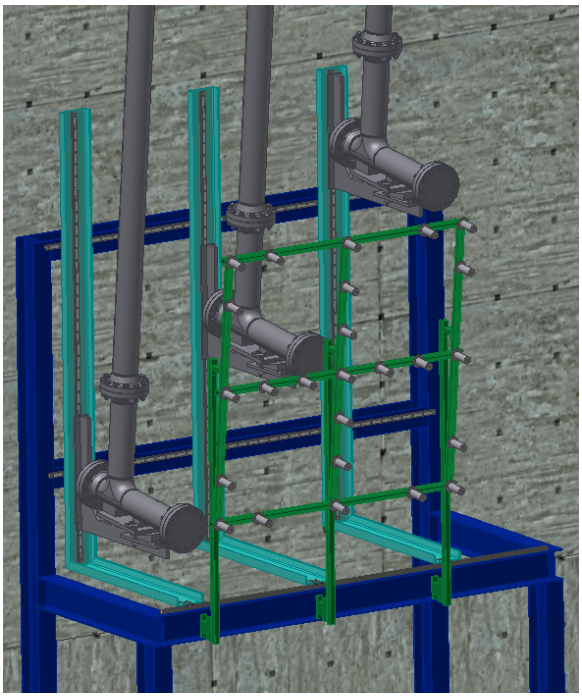

Figure 2–20: The layout of one of the muon Cherenkov counters behind the rear of the absorber.

One possible background is transition radiation, which occurs when a charged particle moves between materials with different indices of refraction. This process can generate light in the visible region, and it can occur even when there is a vacuum inside the gas Cherenkov system. Figure 2–21 also shows that the transition radiation emitted from the mirror surfaces is at least two orders of magnitude lower than the Cherenkov light yield and thus does not introduce a significant background.

A standalone Geant4 [16] simulation for a proposed gas Cherenkov detector for the LBNE muon monitors was developed to investigate various mirror shapes. Based on this work, a conceptual design has been developed, shown in Figure 2–22. Here the muons enter on the right, Cherenkov photons are produced in a region of a dense gas[†], and the light is bounced off of two mirrors towards a photosensor that sits in a lower-radiation environment. Based on fits to a Geant3 [17] simulation of the muons exiting the absorber, the following angular distribution was used to describe the probability of observing a muon with a given angle θ with respect to the beam axis:

$$Prob(\theta) = A \times \theta e^{\frac{-\theta^2}{2\sigma(p)}} \tag{2.1}$$

where A is an arbitrary normalization and the width, a function of the momentum p, is given by

$$\sigma(p) = 5.903 p^{-0.681}. \tag{2.2}$$

[†]Freon was used in the simulations, but a noble gas is the prime candidate.

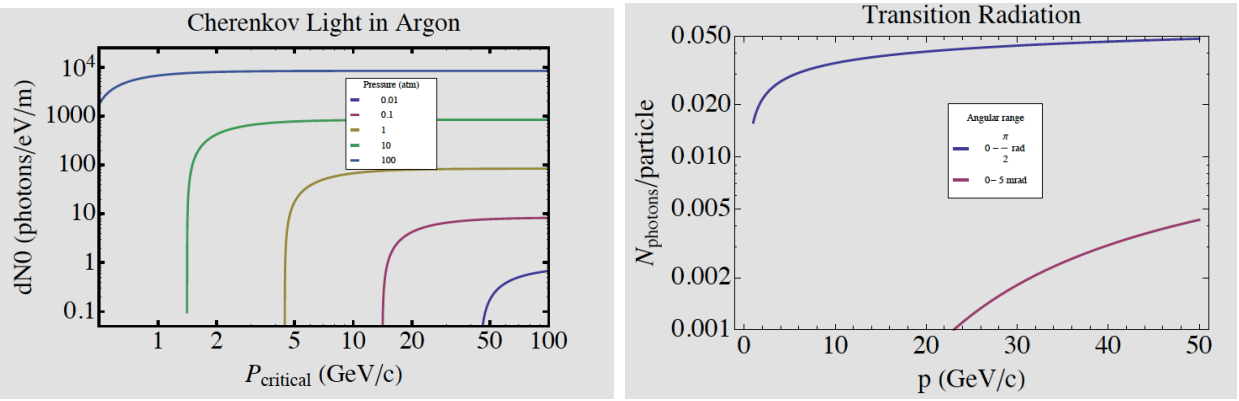

Figure 2–21: The calculated light yields for Cherenkov radiation (left) and transition radiation for muons in argon gas.

Thus, as the momentum increases, $\sigma(p)$ decreases, and the muons become more forward-going.

Several different mirror shapes were examined, including spherical and conical, but much simpler flat mirrors were found to be adequate.

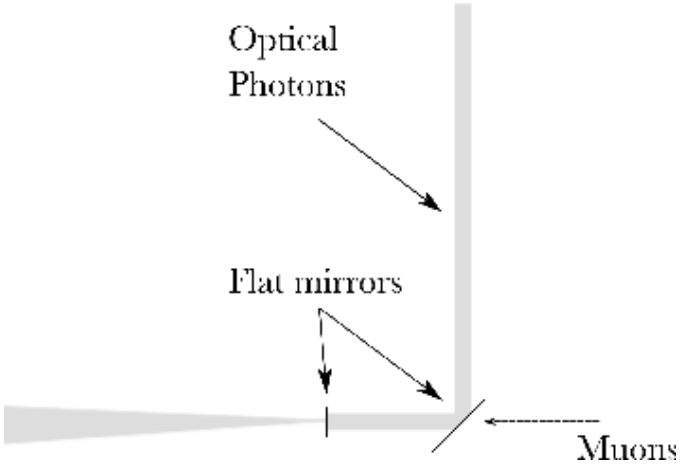

Figure 2–22: Conceptual design for the muon gas Cherenkov detector for LBNE. Muons will travel through an L-shaped pipe filled with a dense gas, and mirrors will direct the optical photons to a photodetector.

Figure 2–23 shows a simulation of the number of photons collected at the photosensor versus muon energy for a range of indices of refraction. Varying the gas density will allow sensitivity of the photon measurements to different parts of the muon-energy spectrum.

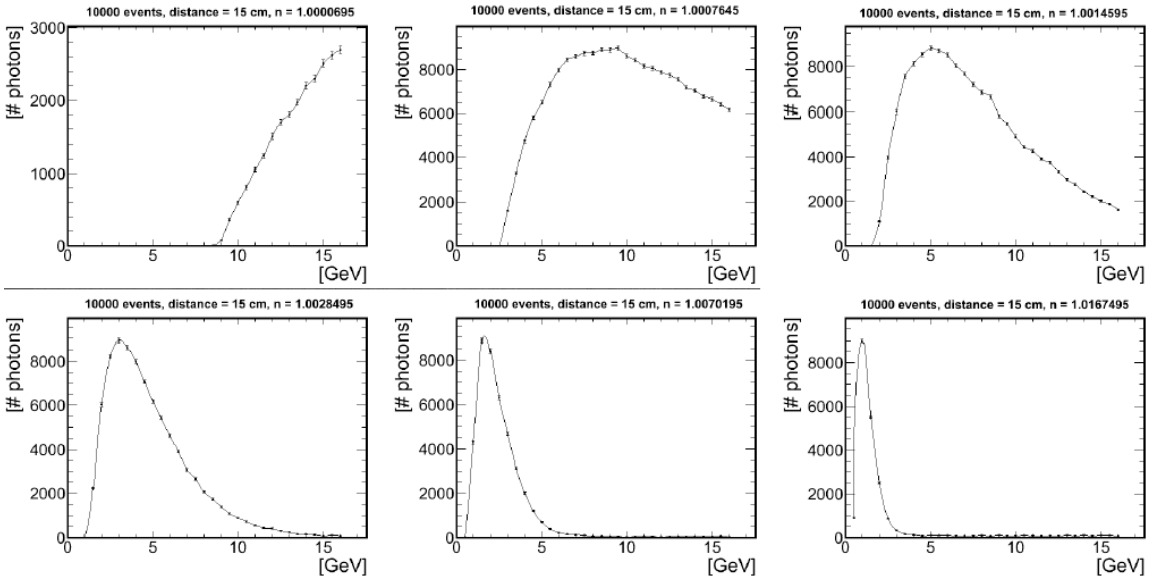

Figure 2–23: The number of photons detected in the photosensor vs. muon energy. Here 10,000 muons have been simulated at each energy. The gas density increases from 0.05 atm in the upper left to 12 atm in the lower right.

2.6.3 Prototype Development and Testing

Because this type of system has not previously been deployed for a muon monitor, significant design work and testing will be required. It will be important to understand the noise and background light from non-Cherenkov sources, such as fluorescence and scintillation in the gas and transition radiation. Some of these items can potentially be examined with cosmic muons. A small prototype system could be tested in the NuMI beam alcoves in 2013, where the goals of the testing would be to understand the linearity of the response and the overall stability of the system, including its sensitivity to atmospheric changes such as the ambient temperature and pressure, and the long term effects of the radiation.

2.6.4 Installation

If this system is included in the LBNE near detector, installation will begin following the installation the stopped muon systems systems. The gas handling system will ideally be located nearby, also on the lower level of the Absorber Hall, as shown in Figure 2–5.

2.6.5 Operation

Because the system will be located in a radiation-controlled environment that will not be accessible during beam operation, it is essential that the electronics and gas handling system

be both robust and remotely operable. Periodic access may be required to the utilities area to replace gas bottles.

3 Near Detector Global DAQ and Computing (WBS 130.03.04)

3.1 Introduction

The purpose of the Global Data Acquisition System (GDAQ) is to collect raw data from each detector in the NDC's Beamline Measurement system (BLM), issue global triggers, add timing data from a global position system (GPS), and build events. Each BLM detector has its own data acquisition system that connects to the GDAQ. Figure 3–1 shows an overview schematic drawing of the GDAQ.

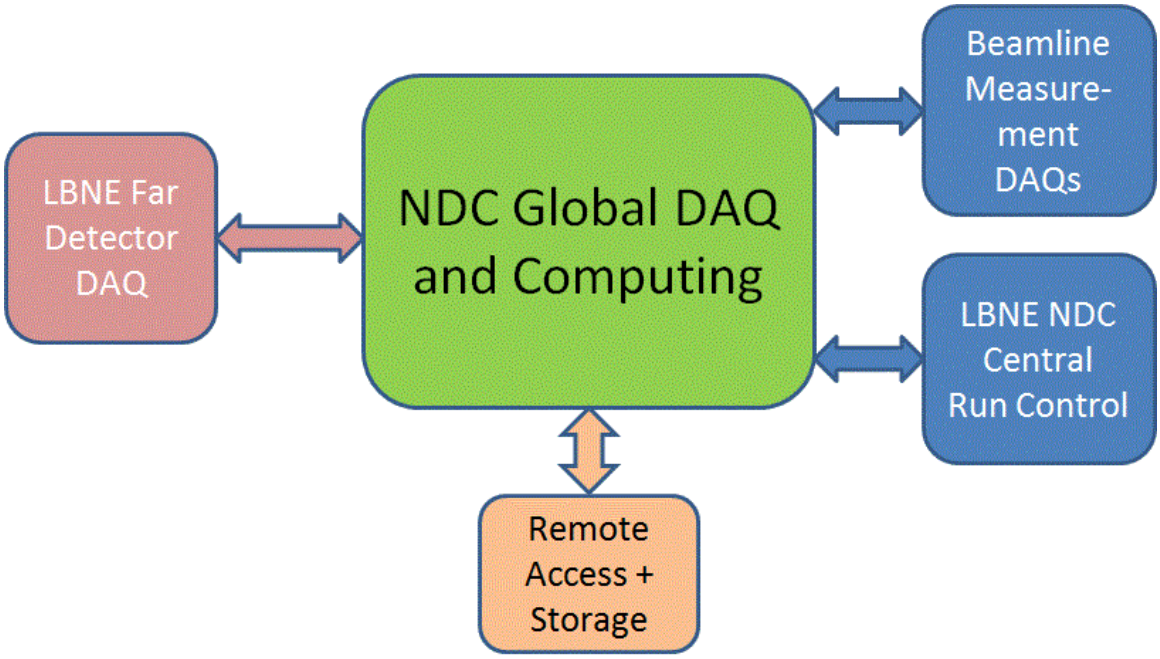

Figure 3–1: Near Detector Complex Global DAQ and Computing (green block) within the LBNE project.

The computing system encompasses two major activities: online computing (the required slow-control systems) and offline computing for further developing our measurement strategy and for simulation work on technical systems.

3.2 Global DAQ

3.2.1 Overview

The Global DAQ (GDAQ) is generally controlled by the LBNE Central Run Control to start and stop runs. It also has its own run control and event builder so that it can run independently of the LBNE Central Run Control, e.g. while the beam is off or for calibration or test runs. It communicates with the beamline detector DAQ systems, and provides two-way trigger processing to and from the beamline detectors. Based on the T2K Near Detector DAQ [18], the proposed system will use Gigabit Ethernet as the primary data-transfer medium.

The GDAQ incorporates a GPS system for precision time-stamping of beam spills and/or detector events and to provide clock and synchronization signals to the individual beamline detector DAQs.

3.2.2 Design Considerations

The detailed GDAQ requirements will have to be developed and specified over time as details of each detector become established; however, there are a number of general system requirements. First, the GDAQ will provide triggers and clock-synchronization signals to the beamline detector DAQs and provide sustainable data-transfer and logging rates via Gigabit Ethernet consistent with the scientific demands of the LBNE experiment. Second, the GDAQ will collect and sort data from the beamline detector DAQs, build global events, format the final event data and save to local storage. Third, the GDAQ will allow inclusion or exclusion of individual detectors from data-taking on a run-by-run basis and allow standalone data-taking of individual detector DAQs for debugging or calibration. Fourth, the GDAQ will provide a local run-control user interface to allow data-taking or debugging independently of LBNE Central run control and will provide an interface for accessing and monitoring online processes and data on a (near) real-time basis for quality control. Fifth, the GDAQ will include a slow-control system with environmental monitoring, and sensor and front-end electronics monitoring. Finally, the GDAQ will allow secure remote access, storage and monitoring capability via firewall to LBNE collaboration member institutions.

3.2.3 Reference Design

The central component of the GDAQ is a computer array serving as the back-end for the Near Detector Complex Global DAQ. It will be a scalable and flexible system that can be expanded or upgraded as needed and as computer technology improves over time. The actual quantity of computers needed for this system and their specifications will depend on the number of channels and expected data rates of the individual detectors, for which the details have not yet been finalized. Using the T2K Near-Detector DAQ experience as a reference, it is safe to assume that a Gigabit Ethernet structure is more than sufficient for the data transmissions between the beamline detectors and the GDAQ.

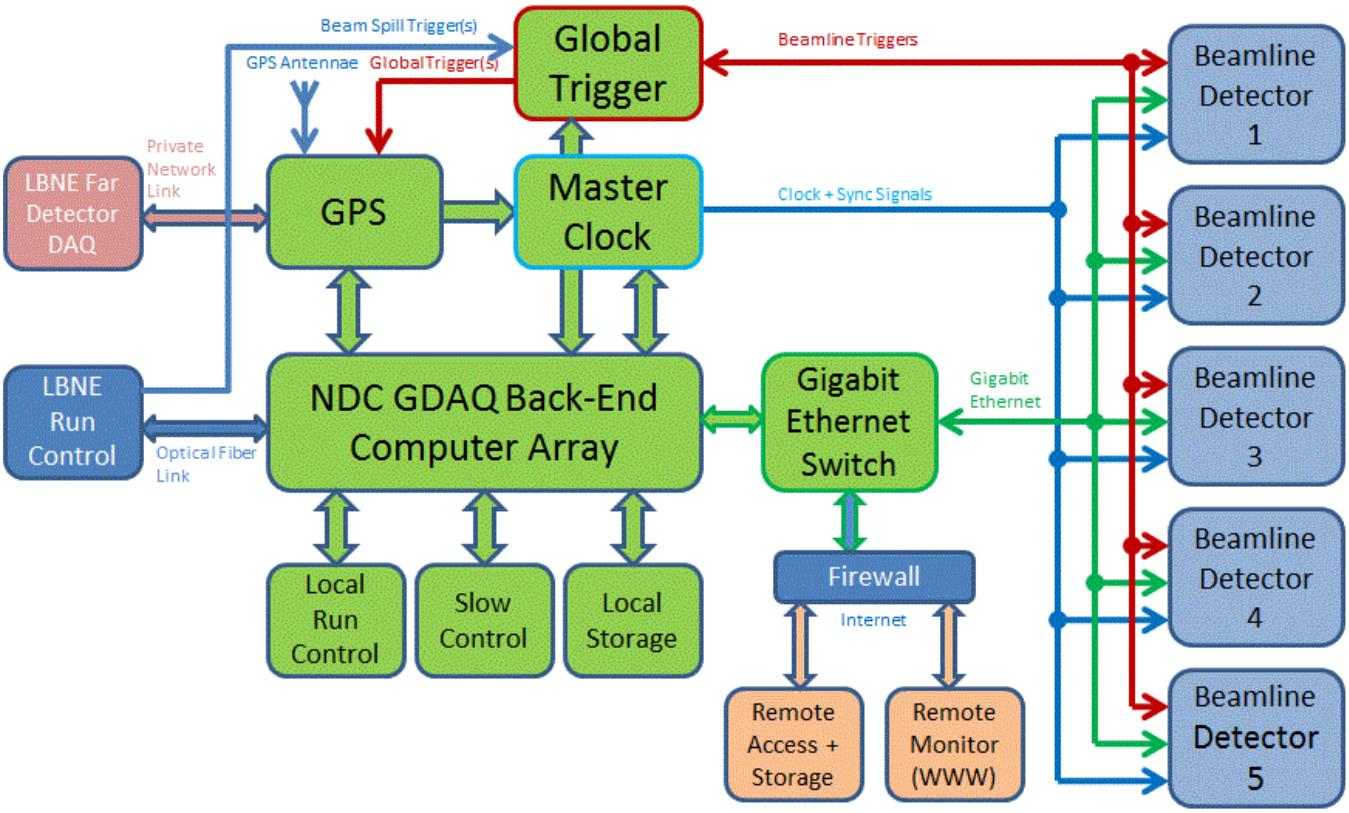

Figure 3–2: Near Detector Global DAQ (GDAQ) block diagram. The green blocks belong to the GDAQ. Other colored blocks are not part of the GDAQ, but shown here for presenting the connections between the GDAQ and other parts of the LBNE project.

Figure 3–2 shows the conceptual design of the GDAQ based on a computer array connected with the beamline detector DAQs via Gigabit Ethernet and other components for triggering and clock synchronization. For starting and stopping runs the LBNE Central Run Control connects to the GDAQ via optical fiber. A GPS subsystem is an integral part of the GDAQ; it provides precision time stamps of each global-trigger event. As an option, the GPS timing data can be transferred to the LBNE Far Detector via a private network (fiber) link to allow

real-time processing of LBNE beam data with Far Detector data – as it is done at T2K with T2K's beamline (and near detector) and Super–Kamiokande as T2K's Far Detector.

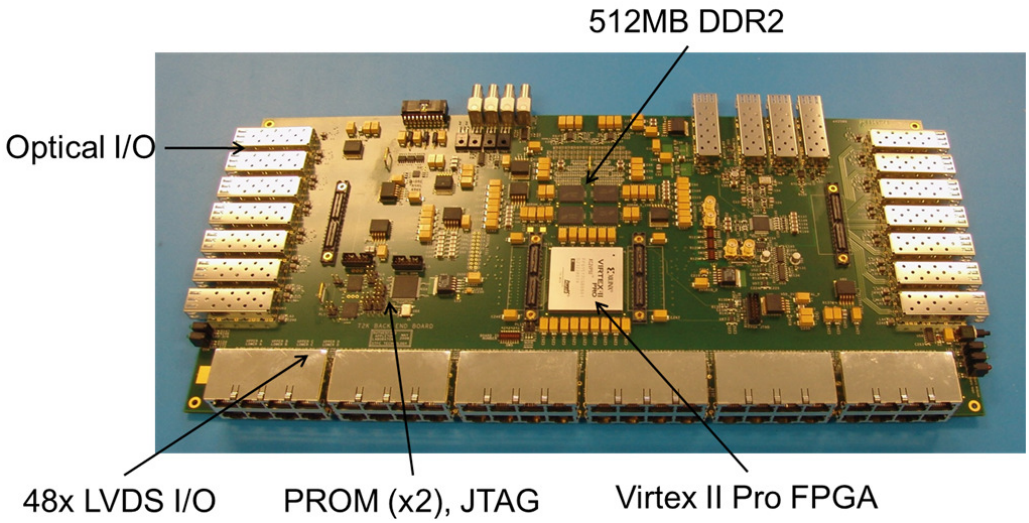

Figure 3–3: [DAQ back-end module designed for T2K ND280 DAQ] DAQ back-end module designed for T2K ND280 DAQ, allowing four selectable functions via FPGA firmware.

A specially designed Global Trigger electronics module processes beam-spill trigger(s) coming from the LBNE central run control. Then, depending on settings either from the GDAQ local run control or LBNE Central Run Control, it sends back trigger signals to the beamline detector DAQs. The Master Clock module, another specially designed electronics module, provides clock- and time-synchronization signals generated by the GPS system and forwards them to the beamline detector DAQ systems. These two special electronics modules can be made of commercial components based on Field Programmable Gate Arrays (FPGA) that can be programmed with high functional complexity and flexibility. For example, the T2K UK group designed and built a universal back-end board for the ND280 DAQ, shown in Figure 3–3, that used a Xilinx Virtex-II FPGA as its central smart-electronics component. The FPGA firmware was written such that the back-end board could be configured for four selectable functions: master clock, slave clock, global or cosmic trigger, and readout merger.

The GDAQ back-end computer array collects and sorts the data coming from the beamline detector DAQs, then builds the events, includes time stamps from the GPS, formats the event, then saves the result to local storage, e.g. disk arrays.

A local run-control option is added to the GDAQ to allow independent detector runs when the LBNE Central Run Control is not being used, e.g. when the beam is off for maintenance or repair or when detector calibration runs are scheduled. The local run-control system will consist of three or four desktop workstations with monitors and keyboards that can also be used for (near) real-time event displays of several detector sections and online data processing and monitoring.

Slow-control electronics is included in the GDAQ with environmental sensors (temperature, humidity, etc.) to monitor the surroundings and status of the DAQ electronics.

Finally, a firewall between the GDAQ network and outside world allows remote access, monitoring and offline data storage of the GDAQ online system by LBNE collaboration institutes.

3.2.4 Global Position System (GPS) within the GDAQ

The Global Position System (GPS) provides high-precision timestamps to beam-spill events and reference clock and synchronization signals between the GDAQ and all BLM detector DAQs. It plays an important role in the LBNE project for synchronizing neutrino beam data with LBNE Far Detector data and for neutrino time-of-flight (TOF) measurements with high precision. Figure 3–4 shows a block diagram of the GPS subsystem.

The GPS subsystem synchronizes the GDAQ with global Universal Time (UTC) via GPS satellites with 10-ns accuracy or better. The proposed system consists of two GPS receivers from different manufacturers/models for redundancy and double-check. At least one of the GPS receivers will be a dual-band (or even multi-band) CommonView capable Time & Frequency receiver with absolute timing accuracy of 10 ns or better, while the other GPS receiver may be a lower-cost, single-band timing receiver with timing accuracy of 50 ns or better. A cesium frequency reference ("Atomic Clock") will be added as a precision base reference clock for the clock synchronization between the GDAQ and beamline detector DAQs, and to maintain timing precision for short periods in case GPS satellite reception is lost, e.g. from lightning strikes at the antenna.

A custom-made interface electronics module, here called "Local Time Clock" (based on the T2K GPS system) [18], will record and buffer the synchronization and slow data signals from the GPS receivers and cesium frequency reference along with global trigger signals from the LBNE run control, beamline and/or near detectors. A CPU then collects the GPS and trigger data from the Local Time Clock and communicates with the GDAQ via Gigabit Etherhet.

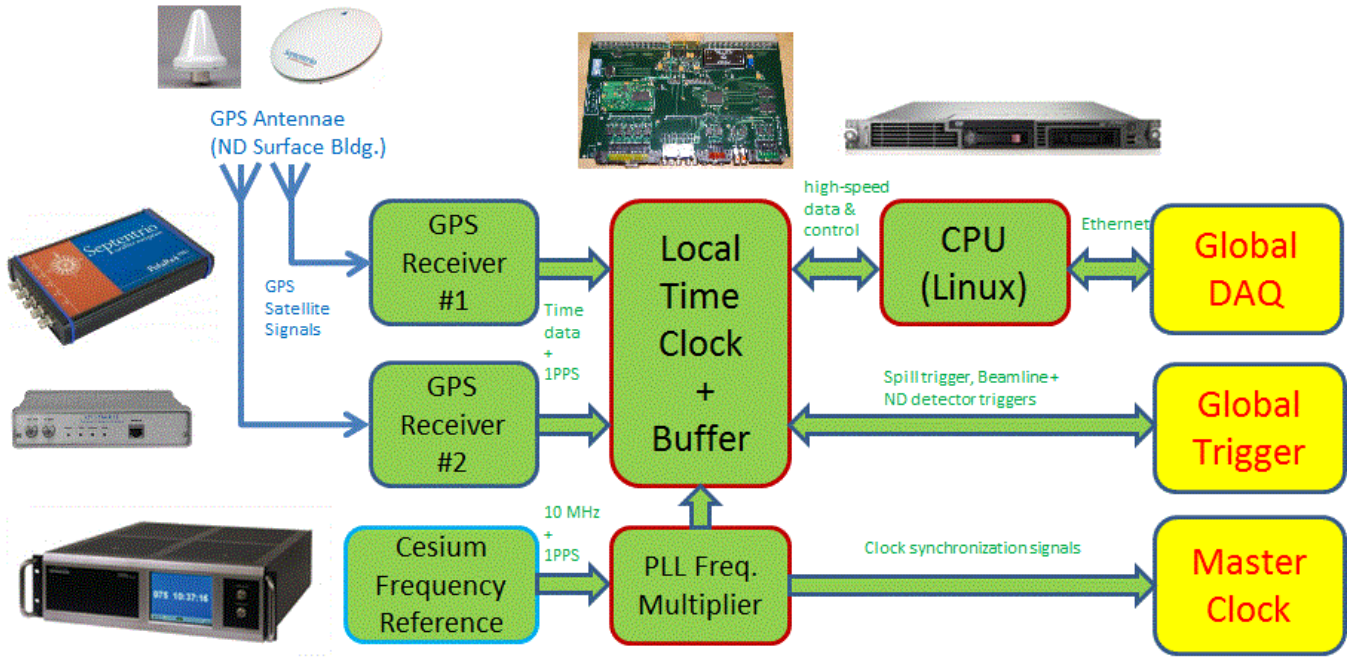

Figure 3–4: Block diagram of the GPS subsystem of the NDC Global DAQ.

3.2.5 Global DAQ and Computing Prototype

A Global DAQ and Computing prototype system is proposed for the preliminary design phase. The goal is to have a platform available for testing and evaluating the principal functionality of a small computer array network with gigabit ethernet switching. It will provide a base system for DAQ software development and allow testing interface options for DAQ data collection from prototype detectors or emulated detector hardware, trigger systems, and clock and time synchronization. Figure 3–5 shows a block diagram of the proposed Global DAQ and Computing Prototype System.

The Global DAQ and Computing hardware will be a scaled-down minimal version of the full Global DAQ system, consisting of the following components:

- one electronics rack with cabling
- four rack-mount computers
- one Gigabit ethernet switch
- two sets of LCD displays, keyboards, mice
- one Uninterruptible Power Supply (UPS)

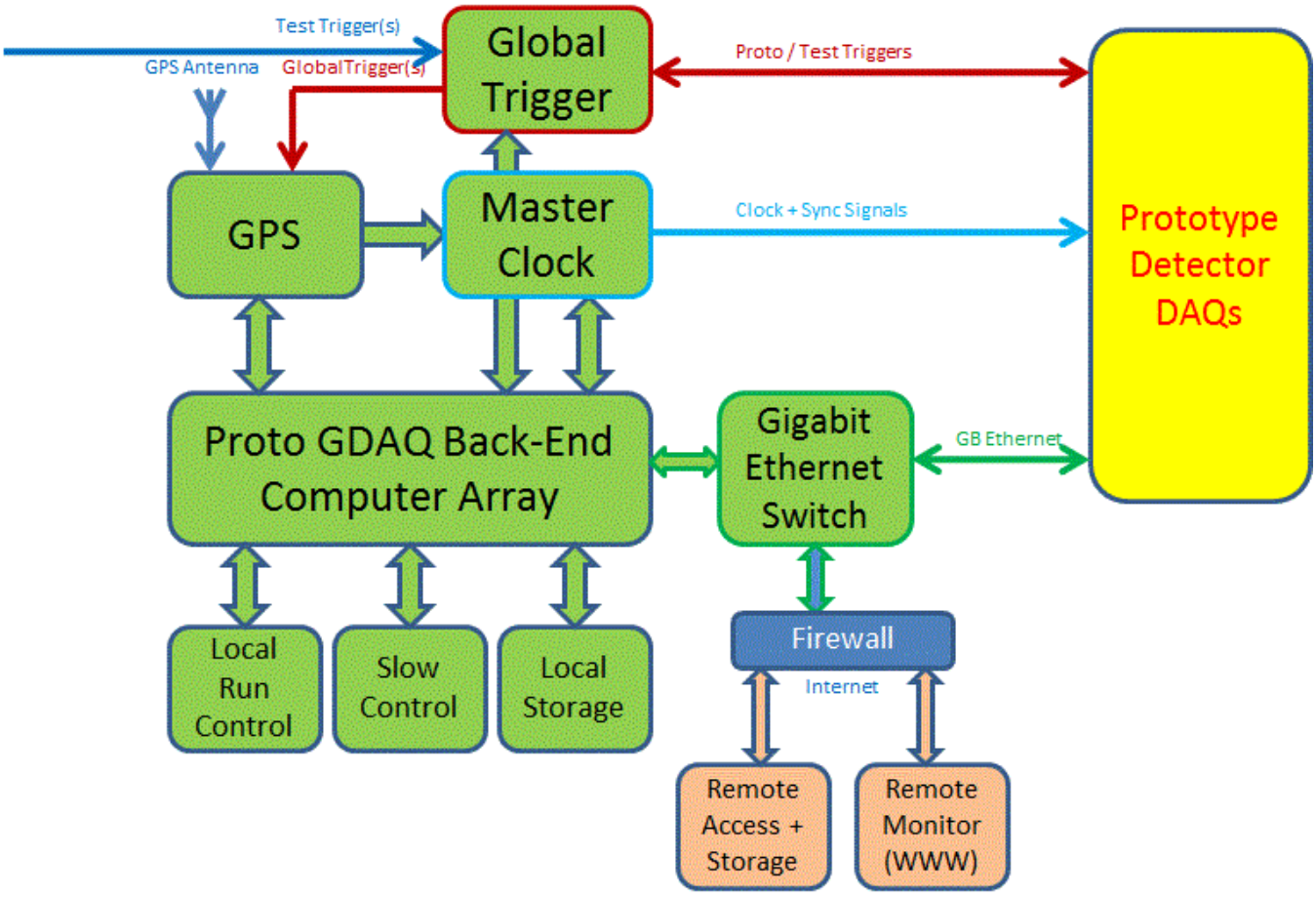

Figure 3–5: Block diagram of proposed Global DAQ and Computing Prototype System, including GPS.

- one slow control interface
- one high-end FPGA development kit for back-end module development
- parts and circuit board service for three prototype back-end modules
- one high-end GPS timing receiver with antenna
- one Rubidium frequency standard module
- one small VME subrack with VME-PCI adapter set
- one custom VME interface (borrowed from T2K GPS system)

3.3 Computing

The computing system encompasses two major activities: online computing (the required slow-control systems) and offline computing which is costed Off-Project, but is important to consider. Offline computing is needed in order to complete the work outlined in the Measurement Strategy described in Section 1.2.1 and the simulation work for the technical systems.

The required slow-control (online) computing systems will be defined as LBNE moves from the conceptual-design to the preliminary-design phase.

For offline computing, resources are currently being provided by Fermilab, LANL and various universities. Project-wide resources are currently being developed at Fermilab and Brookhaven.

4 Measurements at External Facilities

The technical components that would be needed to implement the strategies described in this chapter are outside the scope of the LBNE NDC conceptual design. This information is included in the CDR because it complements the conceptual design and expands the NDC capabilities to more closely meet the mission need without increasing the project cost.

4.1 External Neutrino-Beam Measurements

As discussed in Section 1.2.1, LBNE's strategy for neutrino-beam measurements includes making measurements of the Far Detector response to a known flux of neutrinos, and NuMI is the only appropriate beamline to use for the neutrino source.

To implement this strategy, appropriate detectors will need to be built. A plausible scenario would be a liquid argon TPC detector of 20-30 tons in the current location of the Minerva experiment, in front of the MINOS near detector. In that way, the MINOS near detector could be used to measure the charge of muons exiting the TPC. The TPC would be designed using the same readout techonology that is used in the LBNE Far Detector. Once an optimal detector arrangement is determined, LBNE would use the same beam simulation and same muon measurements to apply that knowledge to the LBNE beam and Far Detector.

4.2 External Hadron-Production Measurements

Uncertainties on hadron production translate into uncertainties in the neutrino fluxes in the LBNE Far Detector, since the hadrons decay into neutrinos in the decay pipe. Therefore, the accuracy to which the neutrino flux must be known at the Far Detector directly determines the required accuracy of the hadron-production measurements, since the LBNE conceptual design does not include a near neutrino detector. This chapter outlines the LBNE strategy for augmenting the capabilities of the BLM with external measurements of secondary-beam particles.

4.3 Background

A complete knowledge of the momenta and decay points of the kaons, pions and muons would be sufficient to completely predict the un-oscillated flux of neutrinos at the Near and Far Detector locations. This would require knowledge of:

- the phase-space distribution of the initial proton beam
- details of all materials present in the target, horn and decay pipe areas
- the electromagnetic focusing characteristics of the magnetic horn
- the detailed development of the hadron cascade, spawned by the initial proton, that passes through the target/horn/decay pipe
- the meson-to-neutrino decay rates

With careful engineering design and careful control of the materials in the target area, all of these items can be simulated accurately except hadronic cascades in the target, horn and decay pipe. The simulation of the hadronic cascade requires accurate knowledge of the hadron scattering cross sections, for which there are no first-principle calculations. These cross sections must therefore rely on models, which in turn require hadron-production measurements that span particle type, particle energy and the various materials found in the target, horn and decay pipe.

At the present time, a sufficient body of hadron-production measurements does not exist to achieve LBNE's desired accuracy of 4-5%, as determined by the irreducible error on the statistical uncertainty for the appearance-measurement background, although this is expected to improve over time. As the BLM system described in Chapter 2 cannot meet this requirement alone, a near-far comparison will be more complicated than in certain other neutrino-oscillation experiments, e.g., MINOS experiment [5].

4.4 Strategy

The current approach is to rely on measurements made externally (outside the scope of LBNE) to calibrate detector response and flux simulations, and to relate these measurements to LBNE. This would be done through the use of a common simulation code and through measurements of tertiary muons in both LBNE and the external facility, using nearly identical tertiary muon-measurement systems.

In order to keep the uncertainty in the near/far event-rate ratio from being limited by systematic uncertainties in the flux, the LBNE flux simulation must be accurate at the 4-5% level. Efforts at this stage are intended to understand the effect of the uncertainties in hadron-production in the beamline on overall LBNE sensitivities, to determine what further measurements may be needed by LBNE and to estimate their potential cost to the Project.

The measurements that LBNE would require from an external facility begin with the primary hadron-production cross sections in the proton-target material, followed by similar studies in thick targets, and finally hadron yields after passage through the complete target and focusing-horn system. In addition, hadron-interaction cross sections on materials in the decay pipe and absorber can be important in flux calculations.

External hadron-production measurements are expected to play a critical role once the Far Detector has accumulated sufficient statistics toward the end of the running period to make systematic errors on the flux a dominant source of error in the oscillation measurement.

4.5 Use of External Facilities for Measurements

Historically, a number of hadron-production experiments have contributed directly to the outcome of neutrino experiments by measuring meson production from the proton targets used by those experiments, and hence providing a constraint on their neutrino fluxes. For example, the HARP data[19] contributed directly to MiniBooNE and the SPY[20] experiment contributed directly to NOMAD. Since their contributions were crucial to those neutrino experiments, it is also expected that LBNE will require some dedicated hadron-production measurements. In the future, the MIPP experiment at Fermilab is planning to contribute its measurements to the NOvA experiment, and the NA61 experiment[21] is contributing to the T2K experiment.

The most suitable apparatus for LBNE's hadron-production measurements is the collection of equipment and detectors used by the MIPP experiment at Fermilab [22]. A full suite of LBNE-related hadron-production measurements would require the installation of the LBNE horn-focusing elements and associated power supplies in front of a future incarnation of MIPP in the meson area at Fermilab. This kind of effort could be within the scope of the LBNE Project and could be postponed until after LBNE construction or even after LBNE operations have stopped.

A proposal for using the NA61 experiment, see Figure 4–1, is also being developed since it is currently operating in the H2 beamline at CERN. NA61 does not have the complete suite of particle identification that MIPP does, but it could provide very useful hadron-production data for predicting neutrino fluxes at LBNE. A pilot run of 120 GeV/c protons interacting on a thin 4% graphite target was taken by NA61 during July, 2012. That run is in the process of being analyzed and will explore the capabilities of the NA61 experiment for LBNE purposes.

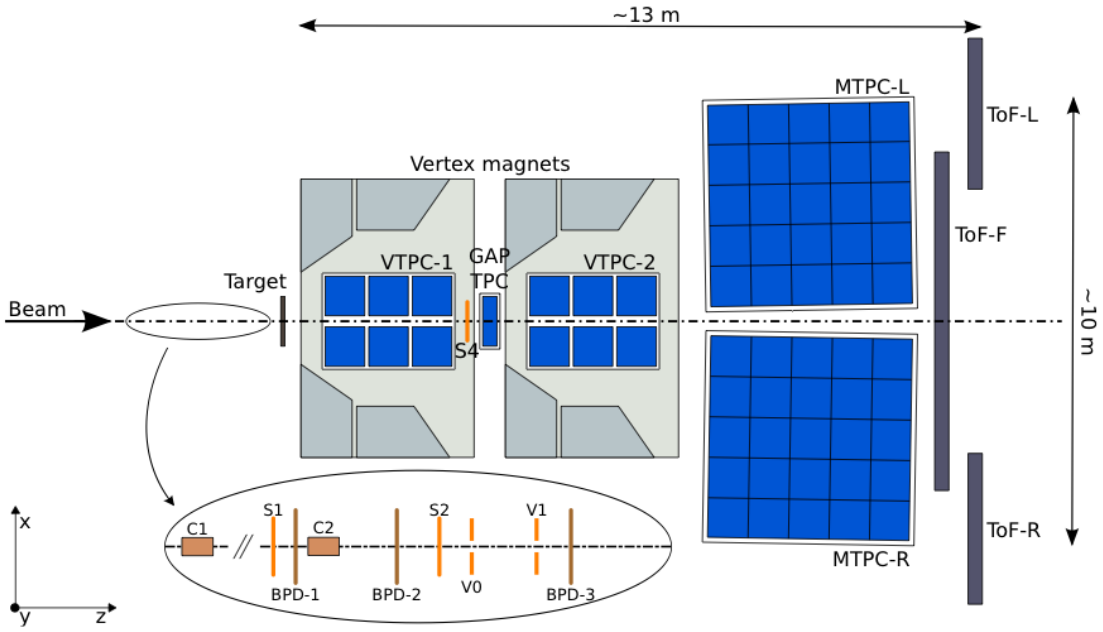

Figure 4–1: A schematic drawing of the CERN NA61 detector, a hadron production and heavy ion experiment designed to measure hadrons over a large part of the relevant phase for neutrino experiments. The TPCs, shown in blue, can separate pions from protons and kaons.

References

[1] Particle Physics Project Prioritization Panel, "US Particle Physics: Scientific Opportunities; A Strategic Plan for the Next Ten Years," 2008. http://science.energy.gov/~/media/hep/pdf/files/pdfs/p5_report_06022008.pdf.

[2] T. Akiri and others, "The 2010 Interim Report of the Long Baseline Neutrino Experiment Collaboration Physics Working Groups." arXiv:1110.6249.

[3] LBNE Project Office, "LBNE Project Management Plan," tech. rep., FNAL, 2011. LBNE Doc 2453.

[4] "Near Detectors Requirements Documentation," tech. rep. LBNE Doc 5579 http://lbne2-docdb.fnal.gov:8080/cgi-bin/ShowDocument?docid=5579.

[5] MINOS Collaboration, "Measurement of Neutrino Oscillations with the MINOS Detectors in the NuMI Beam," *Phys.Rev.Lett.*, no. 101:131802, 2008.

[6] S. Kopp *et al.*, "Secondary beam monitors for the NuMI facility at FNAL," *Nucl. Instrum. Meth.*, vol. A568, pp. 503–519, 2006.

[7] M. H. Ahn *et al.*, "Measurement of Neutrino Oscillation by the K2K Experiment," *Phys. Rev.*, vol. D74, p. 072003, 2006.

[8] T. Maruyama, *First Observation of Accelerator Origin Neutrino Beam After Passing Through 250km of Earth.* PhD thesis, Tohuku University, 2000.

[9] K. Matsuoka *et al.*, "Development and production of the ionization chamber for the T2K muon monitor," *Nucl. Instrum. Meth.*, vol. A623, pp. 385–387, 2010.

[10] H. Kubo *et al.*, "Development of the muon beam monitor for the T2K Long Baseline Neutrino Oscillation experiment," *2008 IEEE Nuclear Science Symposium Proceedings*, pp. 2315–2318, 2008.

[11] D. Meier *et al.*, "Proton irradiation of CVD diamond detectors for high-luminosity experiments at the LHC," *Nucl. Instrum. Meth.*, vol. A426, p. 173, 1999.

[12] K. Hiraide, "Muon Monitoring Using the Decay Electrons," in *4th Workshop on Neutrino Beams and Instrumentation (NBI2003)*, 2003.

[13] Y. Semertzidis and F. Farley, "Effect of light flash on photocathodes," *Nucl. Instrum. Meth.*, vol. A394, p. 7, 1997.

[14] J. Ouyang and W. Earle, "Muon g-2 note no. 202," tech. rep., BNL, 1994.

[15] "GNUMI NuMI Beamline Simulation Code." `http://www.hep.utexas.edu/numi/beamMC/MC-code.html`.

[16] S. Agostinelli *et al.*, "GEANT4 — A Simulation Toolkit," *Nucl. Instrum. Methods*, vol. A, no. 506, pp. 250–303, 2003.

[17] R. Brun, F. Bruyant, M. Maire, A. C. McPherson, and P. Zanarini, "GEANT3." CERN-DD-EE-84-1.

[18] M. Thorpe *et al.*, "The T2K Near Detector Data Acquisition Systems," *Real Time Conference (RT), 2010 17th IEEE-NPSS*, 2010.

[19] M. Catanesi *et al.*, "Measurement of the production cross-section of positive pions in p-Al collisions at 12.9-GeV/c," *Nucl.Phys.*, vol. B732, pp. 1–45, 2006.

[20] G. Ambrosini *et al.*, "Pion yield from 450-GeV/c protons on beryllium," *Phys.Lett.*, vol. B425, pp. 208–214, 1998.

[21] N. Abgrall *et al.*, "Measurements of Cross Sections and Charged Pion Spectra in Proton-Carbon Interactions at 31 GeV/c," *Phys.Rev.*, vol. C84, p. 034604, 2011.

[22] D. Isenhower *et al.*, "Proposal to upgrade the MIPP experiment," *unpublished*, 2006. hep-ex/0609057.